24. Ozaki, A., Tsunoda, M., Kinoshita, S., and Saura, R. Role of fracture hematoma and periosteum during fracture healing in rats: interaction of fracture hematoma and the periosteum in the initial step of the healing process. J Orthop Sci **5,** 64, 2000.
25. Utvag, S.E., Grundnes, O., and Reikeras, O. Effects of degrees of reaming on healing of segmental fractures in rats. J Orthop Trauma **12,** 192, 1998.
26. Yamamoto, M., Takahashi, Y., and Tabata, Y. Controlled release by biodegradable hydrogyels enhances the ectopic bone formation of bone morphogenetic protein. Biomaterials **24,** 4375, 2003.
27. Tabata, Y., Nagano, A., Muniruzzaman, M., and Ikada, Y. *In vitro* sorption and desorption of basic fibroblast growth factor from biodegradable hydrogels. Biomaterials **19,** 1781, 1998.
28. Ozeki, M., and Tabata, Y. *In vivo* degradability of hydrogels prepared from different gelatins by various cross-linking methods. J Biomater Sci Polym Ed **16,** 549, 2005.
29. Otsuru, S., Tamai, K., Yamazaki, T., Yoshikawa, H., and Kaneda, Y. Circulating bone marrow-derived osteoblast progenitor cells are recruited to the bone-forming site by the CXCR4/stromal cell-derived factor-1 pathway. Stem Cells **26,** 223, 2008.
30. Okabe, M., Ikawa, M., Kominami, K., Nakanishi, T., and Nishimune, Y. Green mice as a source of ubiquitous green cells. FEBS Lett **407,** 313, 1997.
31. Sotobori, T., Ueda, T., Myoui, A., Yoshioka, K., Nakasaki, M., Yoshikawa, H., and Itoh, K. Bone morphogenetic protein-2 promotes the haptotactic migration of murine osteoblastic and osteosarcoma cells by enhancing incorporation of integrin beta1 into lipid rafts. Exp Cell Res **312,** 3927, 2006.
32. Wagner, T.U. Bone morphogenetic protein signaling in stem cells—one signal, many consequences. FEBS J **274,** 2968, 2007.
33. Bessa, P.C., Pedro, A.J., Klosch, B., Nobre, A., van Griensven, M., Reis, R.L., and Casal, M. Osteoinduction in human fat-derived stem cells by recombinant human bone morphogenetic protein-2 produced in *Escherichia coli.* Biotechnol Lett **30,** 15, 2008.
34. Deckers, M.M., van Bezooijen, R.L., van der Horst, G., Hoogendam, J., van Der Bent, C., Papapoulos, S.E., and Lowik, C.W. Bone morphogenetic proteins stimulate angiogenesis through osteoblast-derived vascular endothelial growth factor A. Endocrinology **143,** 1545, 2002.
35. Hay, E., Lemonnier, J., Fromigue, O., and Marie, P.J. Bone morphogenetic protein-2 promotes osteoblast apoptosis through a Smad-independent, protein kinase C-dependent signaling pathway. J Biol Chem **276,** 29028, 2001.
36. Marrony, S., Bassilana, F., Seuwen, K., and Keller, H. Bone morphogenetic protein 2 induces placental growth factor in mesenchymal stem cells. Bone **33,** 426, 2003.
37. Maes, C., Coenegrachts, L., Stockmans, I., Daci, E., Luttun, A., Petryk, A., Gopalakrishnan, R., Moermans, K., Smets, N., Verfaillie, C.M., Carmeliet, P., Bouillon, R., and Carmeliet, G. Placental growth factor mediates mesenchymal cell development, cartilage turnover, and bone remodeling during fracture repair. J Clin Invest **116,** 1230, 2006.
38. Fiedler, J., Leucht, F., Waltenberger, J., Dehio, C., and Brenner, R.E. VEGF-A and PlGF-1 stimulate chemotactic migration of human mesenchymal progenitor cells. Biochem Biophys Res Commun **334,** 561, 2005.

Address correspondence to:
Yasuhiko Tabata, Ph.D., D.Med.Sci., D.Pharm.
Department of Biomaterials
Institute for Frontier Medical Sciences
Kyoto University
53 Kawara-cho Shogoin
Sakyo-ku
Kyoto 6068507
Japan

E-mail: yasuhiko@frontier.kyoto-u.ac.jp

Received: May 13, 2009
Accepted: November 3, 2009
Online Publication Date: December 15, 2009

Journal of Dermatological Science 56 (2009) 188–195

Contents lists available at ScienceDirect

Journal of Dermatological Science

journal homepage: www.intl.elsevierhealth.com/journals/jods

Living skin equivalents constructed using human amnions as a matrix

Lujun Yang [1], Yuji Shirakata [1,*], Sho Tokumaru, Dai Xiuju, Mikiko Tohyama, Yasushi Hanakawa, Satoshi Hirakawa, Koji Sayama, Koji Hashimoto

Department of Dermatology, Ehime University Graduate School of Medicine, Shitsukawa 454, Toon City, Ehime, 791-0295, Japan

ARTICLE INFO

Article history:
Received 17 July 2009
Received in revised form 24 September 2009
Accepted 24 September 2009

Keywords:
Amnion
Living skin equivalent
Mesenchymal interaction
Basement membrane

ABSTRACT

Background: Living skin equivalents (LSEs) are being used to treat burn wounds, skin defects, and chronic wounds, and today, several biomaterials are applied as dermal matrices in LSEs. The amnionic membrane (AM) is known to have useful properties as a dermal matrix and can be used to construct a LSE.
Objective: To develop a new LSE with human AM as the matrix.
Methods: Human AM was de-epithelialized and investigated to determine whether it supported keratinocyte adherence and proliferation, and fibroblast in-growth and proliferation. A new LSE was constructed by seeding keratinocytes on the epithelial side of fibroblast-populated, de-epithelialized AM and was investigated histologically. The LSE was transplanted onto a full-thickness wound on a nude mouse and a histological examination was conducted.
Results: De-epithelialized AM supported the adherence and proliferation of keratinocytes and the in-growth of fibroblasts. The new LSE demonstrated good mechanical properties and revealed good morphology, with a well differentiated epidermis and well developed basement membrane. The LSE grafts survived well on nude mice, showing good morphology.
Conclusion: A LSE with amnions as a matrix exhibited good morphology, low cost, and good mechanical properties and may be useful as a skin substitute for clinical use.

1. Introduction

Living skin equivalents (LSEs) containing well differentiated keratinocytes cultivated on fibroblast-populated dermal substitutes have been used to treat burn wounds, skin defects, chronic wounds, and ulcers [1–3]. The dermal matrix and the fibroblasts in LSEs modulate epidermal growth and differentiation through dynamic interactions [4–6]. Various biomaterials have been used as dermal matrix substitutes, including type I collagen, acellular human dermis, collagen–glycosaminoglycan matrix, human plasma, and fibrin glue [7–11]. However, the search has continued for an ideal matrix that is readily available and inexpensive and supports mesenchymal cell in-growth, improves epidermal cell adherence and proliferation, and has minimal toxicity, low immunogenicity, and good mechanical properties.

Amnions can be readily obtained from cesarean deliveries after screening for viral diseases. Amnions have been used to cover clean partial-thickness wounds and donor sites, and applied as a temporary dressing for freshly excised burns; it has advantages such as pain relief, prevention of infection, maintenance of a moist environment to promote healing, good adherence to wounds, and simple handling [12–17]. Laboratory investigations have revealed that the basement membrane (BM) of amnions shares major BM components with human skin, and the BM zone resembles human skin both morphologically and ultrastucturally [18]. The epithelial side of denuded amnions has been shown to support the proliferation, spreading, and differentiation of corneal, mucous, and bronchial epithelial cells [19–21]. Furthermore, the stroma of amnions can serve as a dermal matrix in which fibroblasts show good adherence and proliferation [22,23]. Limited immunogenicity, along with anti-inflammatory effects and other characteristics, make it a suitable transplantation material for ocular surface reconstruction, and the immune privilege of the amnion makes it a biological immune barrier for xenotransplantation [24–26]. Moreover, amnion procurement and processing are easy and it can be sterilized and preserved at low cost for long periods without obvious architectural changes [27–29].

Considering these characteristics of amnions, in this study, we used amnions as a substratum to construct a LSE. We studied the

* Corresponding author. Tel.: +81 89 960 5350; fax: +81 89 960 5352.
E-mail address: shirakat@m.ehime-u.ac.jp (Y. Shirakata).
[1] Both these authors contributed equally to this work.

0923-1811/$36.00
doi:10.1016/j.jdermsci.2009.09.009

morphology and function of fibroblasts cultured in the stroma of amnions and the morphology of keratinocytes on the epithelial side of de-epithelialized amnions. The LSE was constructed by seeding keratinocytes on fibroblast-infiltrated amnions and was investigated histologically, immunohistochemically, and ultrastructually. The LSE was also investigated *in vivo* by transplantation onto nude mice.

2. Materials and methods

2.1. Cell culture

Normal human epidermal keratinocytes (NHKs) were isolated from healthy human skin and cultured under serum-free conditions, as described previously [30,31]. The cells were used for LSE cultures in their fourth passage. Fibroblasts were isolated from healthy human skin and cultured in Dulbecco's modified Eagle's medium (DMEM; Gibco, Grand Island, NY, USA) supplemented with 10% fetal calf serum (FCS). Fifth-passage cells were used to construct the LSEs.

All procedures that involved human subjects received prior approval from the ethics committee of Ehime University School of Medicine, Toon City, Ehime, Japan. All subjects provided written informed consent.

2.2. Preparation of de-epithelialized amnions

Human amniotic membrane (AM) was obtained at cesarean section. Under sterile conditions, the AM was washed with sterile phosphate-buffered saline (PBS), deprived of the spongy layer, and stored at −80 °C in 12% dimethyl sulfoxide (DMSO) in PBS. Before use, the AM was thawed, washed with PBS three times, and cut into 2.5 cm × 2.5 cm pieces. The epithelial cells were removed from the AM by incubating it in 0.02% ethylenediaminetetraacetic acid (EDTA) at 37 °C for 2 h, and then gently scraping with a cell scraper under a microscope, as previously described [32]. The complete removal of epithelial cells was confirmed using hematoxylin and eosin (H&E) staining.

2.3. De-epithelialized AM for cultivating keratinocytes and dermal fibroblasts

De-epithelialized AM was put on the bottom of a six-well culture plate (Costar; Corning, Corning, NY, USA) with the epithelial side upward, and stabilized by overlaying a stainless steel ring (inner diameter, 20 mm). Keratinocytes (1×10^6 cells) were seeded onto the AM in MCDB 153 II medium. The same number of keratinocytes was seeded in a type I collagen-coated six-well plate (Iwaki; Asahi Techno Glass, Chiba, Japan) of the same area as the AM. Then, 4 h later, the cells were stained with calcein AM (using the Live/Dead Viability/Cytotoxicity Kit; Molecular Probes, Eugene, OR, USA) according to the manufacturer's protocol. The fluorescence was examined and photographed under a phase-contrast microscope (TE-300; Nikon, Tokyo, Japan), coupled with a Nikon pixera digital camera penguin 600 CL. Three days later, the confluent keratinocytes were photographed under the same phase-contrast microscope.

Fibroblasts (5×10^5) were seeded in each well of a six-well culture plate in DMEM supplemented with 10% FCS and 50 μg/mL ascorbic acid. When the cells reached confluence, de-epithelialized AM was placed on the cells, with the stromal side downward, to be in touch with the fibroblasts. The AM was stabilized with a stainless steel ring. At the first and fifth day after AM application, pictures were taken of the fibroblasts on the AM.

We performed at least three independent experiments, which showed similar results. Representative data are shown in the figures.

2.4. Preparation of skin equivalents

Fibroblasts (5×10^5) were seeded in culture inserts (Transwell-COL, membrane pore size, 3 μm, Costar; Corning) and cultured in DMEM supplemented with 10% FCS in a 6-well plate (Costar; Corning). One day later, de-epithelialized AM was put on to the confluent fibroblasts, with the stromal side downward, and stabilized with a stainless steel ring (inner diameter, 20 mm). Five days later, when the fibroblasts had infiltrated the AM stroma (confirmed by phase-contrast microscopy), 2×10^6 keratinocytes in 500 μL MCDB 153 type II medium were seeded in the hole of the stainless steel ring. The keratinocytes were kept submerged in culture for 2 days. Then, the LSE was lifted to provide an air–liquid interface and cornification medium (1:1 mixture of Ham's F-12 and DMEM supplemented with 2% FCS and other supplements, as described previously [33]) was added. This medium was changed every other day.

The LSEs were harvested at day 10 after airlift. For each sample, one part was fixed in 20% formalin and embedded in paraffin for H&E staining, one part was snap-frozen in optimal cutting temperature (OCT) compound for immunofluorescence staining, and one small part was processed for transmission electronic microscopy (TEM). We performed more than 20 experiments, and similar results were obtained. A representative experiment is shown in the figures.

2.5. Histology and immunofluorescence staining

Paraffin-embedded LSE samples were sectioned at 6 μm and stained with H&E. Images were obtained using an Olympus AX80 microscope coupled with an Olympus DP50 digital camera (Olympus, Tokyo, Japan).

For immunofluorescence (IF) staining, frozen sections (7 μm) were first incubated with 0.3% hydrogen peroxide for 30 min to remove endogenous peroxidase activity and then incubated with primary antibodies at appropriate dilutions (Table 1) overnight at 4 °C. The sections were incubated with anti-mouse fluorescein isothiocyanate (FITC) for 30 min at room temperature. Images were obtained using a fluorescence microscope (E6TUW-RFL; Nikon) coupled with an Olympus DP70 digital camera. We performed at least three independent studies, which gave similar results. A representative experiment is shown in the figures.

2.6. Mechanical and handling properties of the living skin equivalent and transplantation on nude mice

A larger LSE was made using a larger culture insert (diameter, 75 mm, membrane pore size, 3 μm, Transwell; Corning), a larger piece of amnions (about 4 cm × 4 cm), and proportionally more fibroblasts and keratinocytes in the same way as described above. At day 7 after airlift, the LSE was harvested and made into a mesh-skin graft with a scalpel and stretched.

The grafting protocol was approved by the ethics committee of Ehime University School of Medicine. Eight-week-old female

Table 1
Details of primary antibodies.

Antibody to	Clone	Dilution	Source
E-cadherin	HECD-1	1:100	TaKaRa
Desmoglein 3	5G11	1:100	Zymed
Keratin 14	LL002	1:100	NeoMarkers
Keratin 10	LHP1	1:100	NeoMarkers
Integrin β4	3E1	1:100	Chemicon
Integrin α2	P1E6	1:100	Chemicon
Collagen type VII	LH7.2	1:100	NeoMarkers
Collagen type IV	2311C3	1:200	Chemicon
Laminin 5	GB3	1:100	Sera-lab

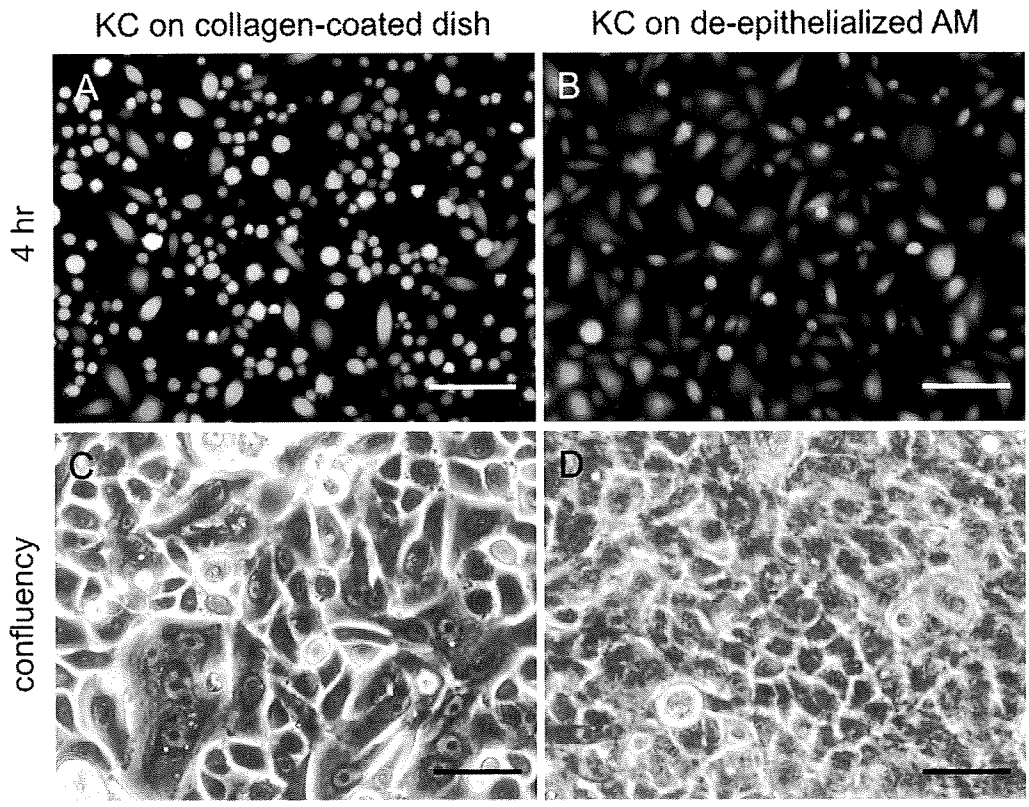

Fig. 1. Morphology of keratinocytes on de-epithelialized amnions. Keratinocytes were seeded onto a type I collagen-coated dish (A and C) or the epidermal side of de-epithelialized amnions (B and D). Four hours after seeding, the plasma of cells was stained with calcein AM of the Live/Dead Viability/Cytotoxicity Kit and photographed (A and B). Three days later, the cells reached confluence and were photographed under a phase-contrast microscope (C and D). Bars are 50 μm.

BALB/cAJc1-nu nude mice were anesthetized with intraperitoneal injection of 0.3 mL Avertin (1.25% tribromoethanol, 2.5% 2-methyl-2-butanol solution). A 1.5 cm × 1.5 cm full-thickness wound was created on the back of each mouse using scissors; then a piece of LSE of matching size (7 days after airlift) was grafted onto the wound and covered with a transparent film. Fourteen days after transplantation, pictures of the grafts were taken and the grafts were harvested and processed for H&E staining. We performed at least three independent studies, which gave similar results. A representative experiment is shown in the figures.

2.7. Transmission electron microscopy

Specimens were fixed in 0.1% tannic acid containing 2.5% glutaraldehyde in 0.1 M phosphate buffer (pH 7.4) for 2 h, washed with phosphate buffer, post-fixed with 1% osmium tetroxide in phosphate buffer for 2 h, washed with 0.25 M sucrose solution, dehydrated in a graded series of ethanols, and embedded in an Epon resin mixture. Ultrathin sections (<60–80 nm) were prepared using an Ultracut S (Leica, Solms, Germany) double-stained with uranyl acetate and lead citrate, and examined with a

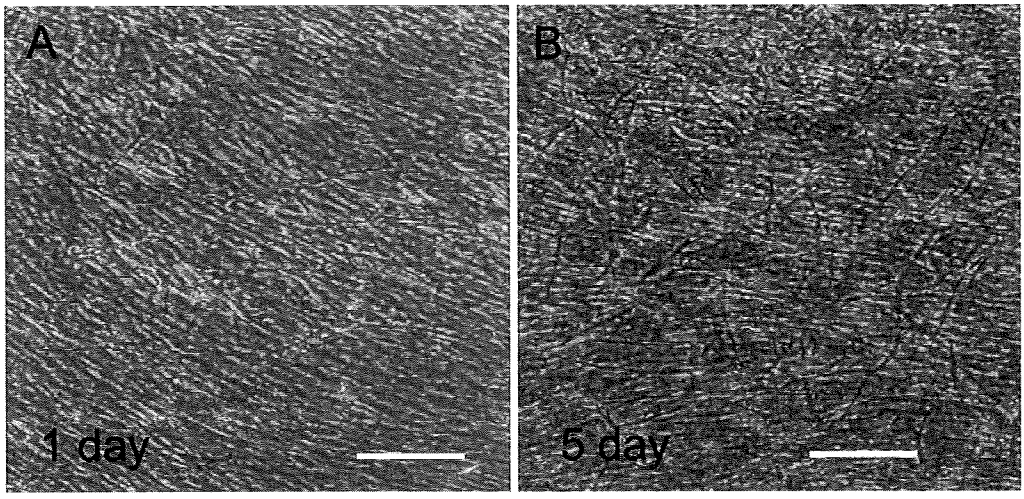

Fig. 2. Morphology of fibroblasts in the stroma of amnions. De-epithelialized amnions were placed on confluent fibroblasts with the stromal side downward. One day (A) or 5 days (B) later, the morphology of fibroblasts was examined. Bars are 50 μm.

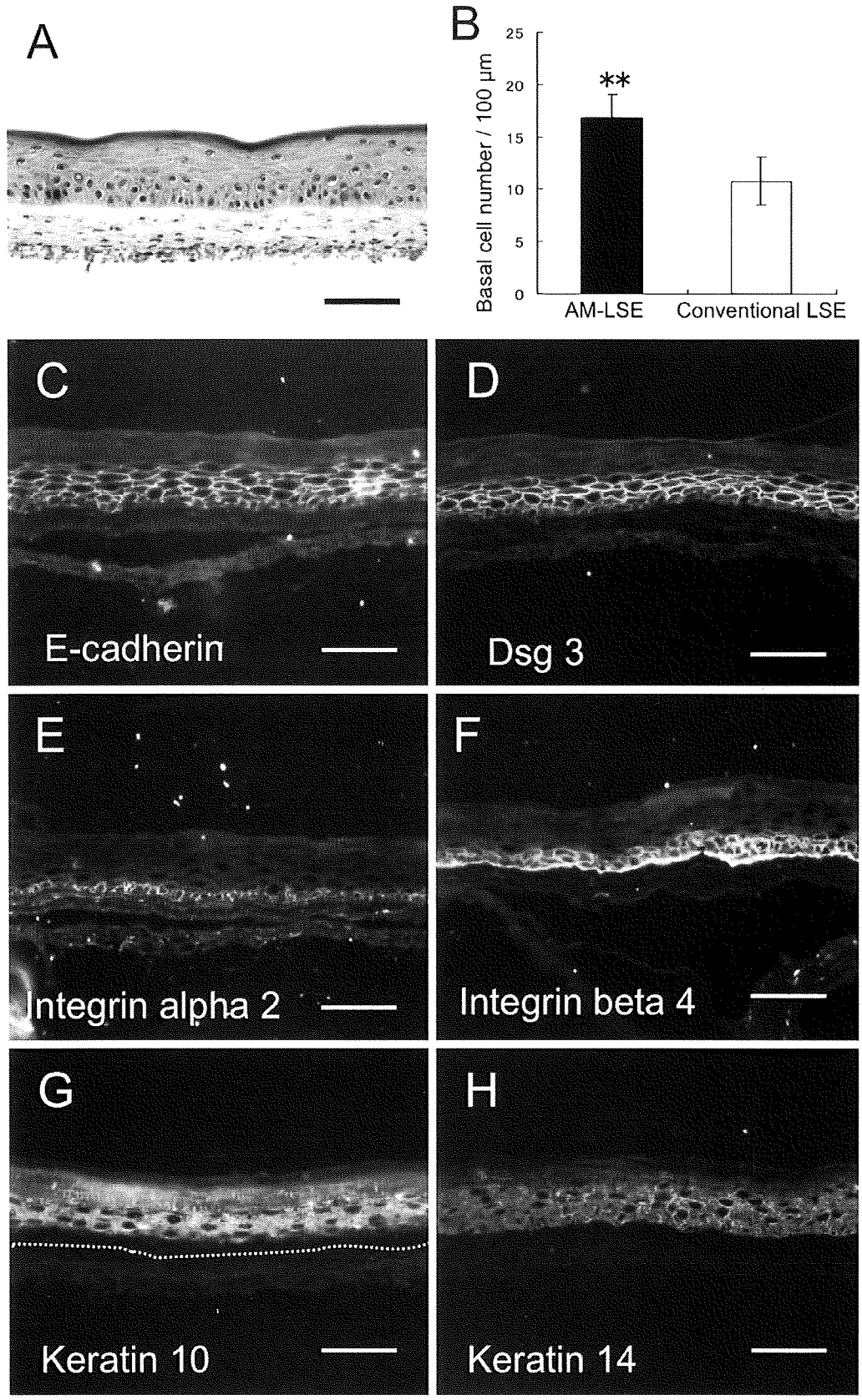

Fig. 3. Morphology of living skin equivalents and the expression of cell–cell junction proteins, integrins, and keratins. Keratinocytes were seeded onto fibroblast-infiltrated de-epithelialized amnions to create living skin equivalents (LSEs). Ten days after airlift, the LSEs were harvested. The histological morphology is indicated by H&E staining (A). The basal cell number per 100 μm at dermal-epidermal junction was counted, and compared with a conventional LSE built with type I collagen. $^{**}p < 0.05$ (B). The cell–cell junction is shown by immunofluorescence (IF) staining of E-cadherin (C) and Dsg 3 (D). The polarization of epidermal cells is indicated by IF staining of integrin α2 (E) and β4 (F). The differentiation and proliferation status of the epidermis are shown by the expressions of keratin 10 (G) and keratin 14 (H). Bars are 50 μm.

transmission electron microscope (JEM-1230; JEOL, Tokyo, Japan) at 80 kV. We performed at least three independent studies and confirmed similar results. A representative experiment is shown in the figures.

3. Results

3.1. De-epithelialized amnions supported keratinocyte and fibroblast growth

Four hours after the seeding of keratinocytes, the cell plasma was stained with calcein AM and the morphology of the keratinocytes was observed. In amnions, most of the cells became larger and adopted a spindle-like shape (Fig. 1B) in comparison with the small and round cells on the type I collagen-coated dish (Fig. 1A). At day 3, when the cells reached confluence, keratinocytes on de-epithelialized amnions appeared more compactly arranged with a pavement stonelike morphology (Fig. 1D), while the cells on the type I collagen were larger and appeared irregular (Fig. 1C).

The amnions were overlaid with the stromal side downward on confluent fibroblasts. Under phase-contrast microscopy, we observed morphological changes in the fibroblasts in the amnions. One day after amnion application, very few fibroblasts sprouted into the amnions, with thin and long dendritic branches (Fig. 2A). At day 5, more fibroblasts moved into the stroma of the amnions and formed a complex network of dendritic branches (Fig. 2B).

3.2. A well differentiated epidermis formed on de-epithelialized amnion with a well developed basement membrane

At day 10 after airlift, the LSEs were harvested and processed for histological, immunohistochemical, and ultrastructural studies. A multilayered epidermis formed on de-epithelialized amnions and epidermal stratification was well organized (Fig. 3A). The basal cells were cuboid, small, and compactly aligned along the AM, with clear demarcation. The number of basal cells on dermal–epidermal junction is significantly higher than that of a conventional LSE made by seeding keratinocytes on fibroblast-populated type I collagen gel (Fig. 3B) [32,33]. The spinous layer, granular layer, and stratum corneum were also clearly identified. The fibroblasts infiltrated deeply into the stroma of the amnion except for a thin acellular zone, which separated the epidermis from the underlying fibroblast-infiltrated substratum (Fig. 3A). Cell–cell junctions were well developed in the epidermis, as shown by the expression of

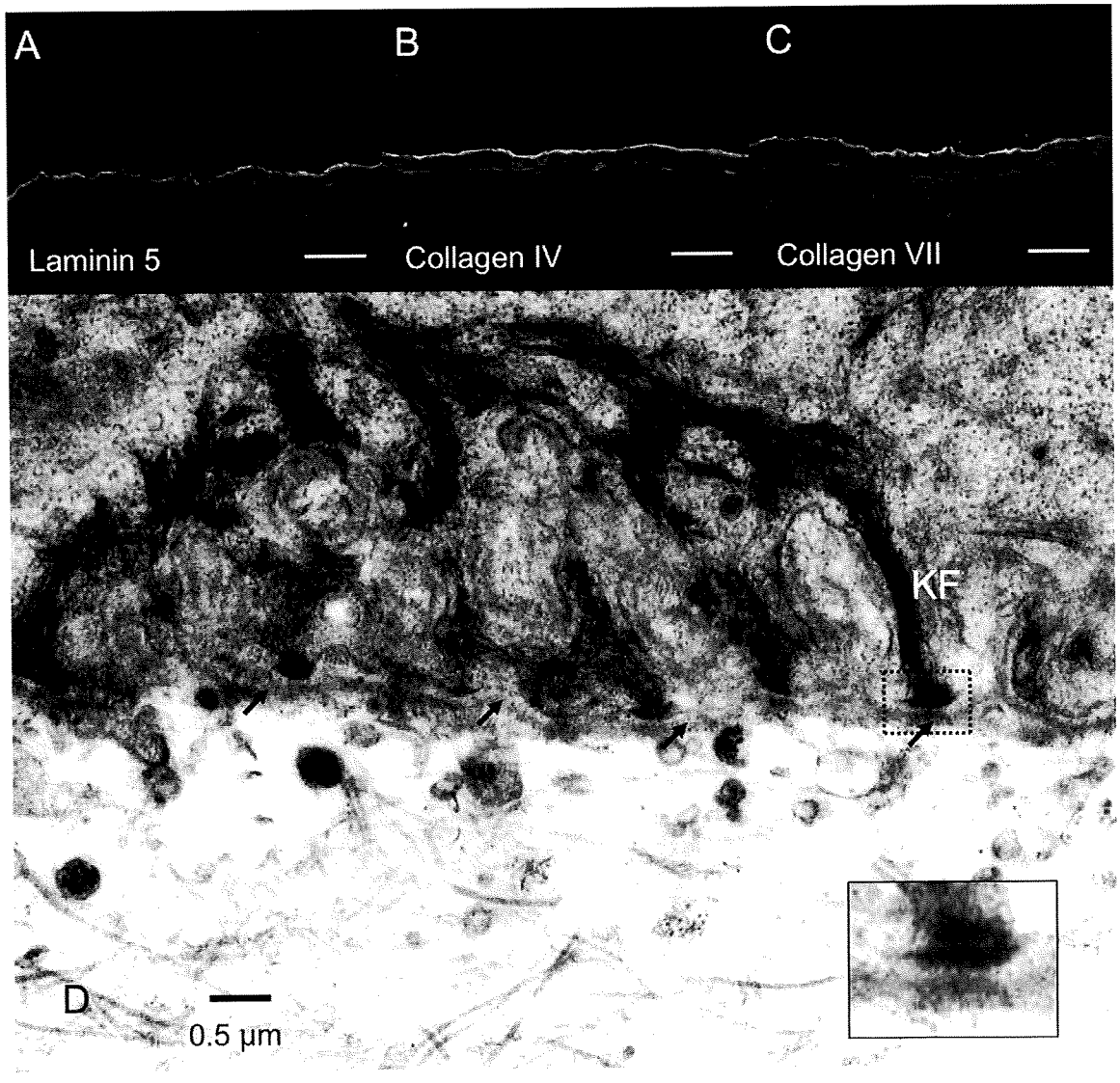

Fig. 4. Basement membrane development in living skin equivalents. On frozen sections of living skin equivalent samples, the expression of laminin 5 (A), type IV collagen (B), and type VII collagen (C) were determined by immunofluorescence staining with the respective monoclonal antibodies. Transmission electron microscopy revealed a continuous lamina densa (arrows in D) and well developed hemidesmosomes (inset in D). KF, keratin filaments. Bars are 50 μm in A, B, and C and 0.5 μm in D.

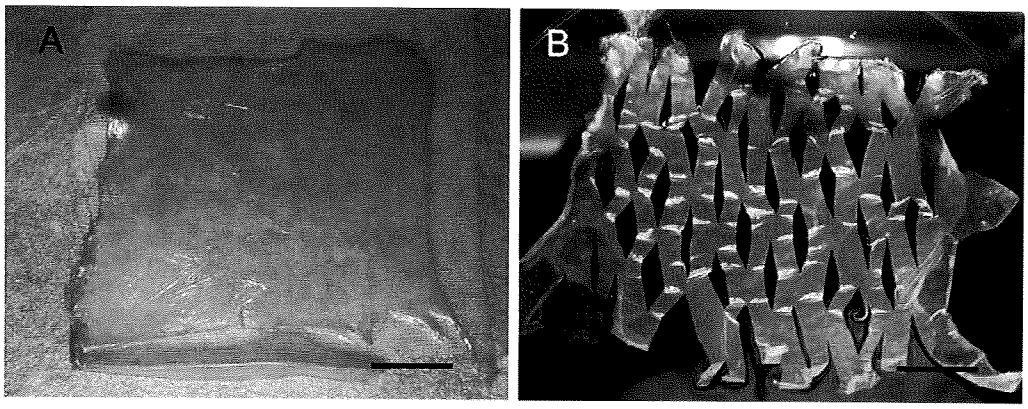

Fig. 5. A large living skin equivalent showed good mechanical properties. An amnion living skin equivalent (LSE) was made with an amnion of 4 × 4 cm. At day 7 after airlift, the LSE was lifted and made into a mesh-skin graft with a scalpel. The LSE was photographed before (A) and after (B) the mesh-skin graft processing. Bars are 1 cm.

E-cadherin and desmoglein 3 (Dsg 3) around each cell (Fig. 3C and D). We also noticed polarization of the epidermal cells, as shown by the distribution of integrin alpha 2 and integrin beta 4, which was restricted to the basal and lower suprabasal layer of the epidermis (Fig. 3E and F). The distribution of keratin 10 extended from the suprabasal layer to the stratum corneum (Fig. 3G), indicating the differentiated status of the keratinocytes. Keratin 14 was seen in the basal and suprabasal layers, indicating the proliferative status of the cells (Fig. 3H).

Considering BM development is important when investigating a cultivated LSE. IF staining revealed linear and compact deposition of the major BM proteins, laminin 5, and types IV and VII collagen at the epidermal–dermal junction (Fig. 4A–C). The development of the BM zone was further examined using transmission electron microscopy (TEM). A continuous lamina densa was formed along the plasma membrane of the keratinocytes, with many hemidesmosomes. The hemidesmosomes were well developed structurally, with inner and outer plaques clearly distinguished; keratin filaments were connected to the inner plaques (Fig. 4D).

3.3. Amnion LSEs showed good mechanical and handling properties

At day 7 after airlift, the large amnion LSE was ready for use, with a yellowish color to the cornified epidermis (Fig. 5A). The LSE was readily lifted from the culture insert and transferred to a culture dish with forceps, without separation of the epidermis and dermis or rupture of the dermal matrix. Furthermore, the amnion LSE was firm enough to tolerate scalpel cutting and could be stretched to prepare a mesh-skin graft (Fig. 5B).

3.4. Amnion LSE graft on nude mice was well vascularized and showed good morphology

Two weeks after transplantation, the grafts had survived on nude mice, with even surfaces and a pink coloration (Fig. 6A). The grafts were harvested and processed for H&E staining. The epidermis was well stratified, with columnar basal cells compactly aligned along the epidermal–dermal junction, round spinous cells and flat granular cells in the upper layers, and a thick stratum corneum on the surface. The amnion could still be distinguished by an acellular zone, which remained uninfiltrated by underlying mesenchymal cells. In the substratum, many small blood vessels were found up to the acellular zone (Fig. 6B).

4. Discussion

In this study, we confirmed that keratinocytes spread and proliferated well on the epithelial side of de-epithelialized amnions, and found that the stroma of amnions supported fibroblast adherence and infiltration. The LSE was constructed by seeding keratinocytes on fibroblast-infiltrated amnions and was investigated *in vitro* and *in vivo*.

Amnions can be de-epithelialized and preserved, with intact basal lamina remaining [34,35]. The exposed BM components of amnions enhance corneal epithelial cell adherence, proliferation, and migration [19]. In this study, we found that normal human

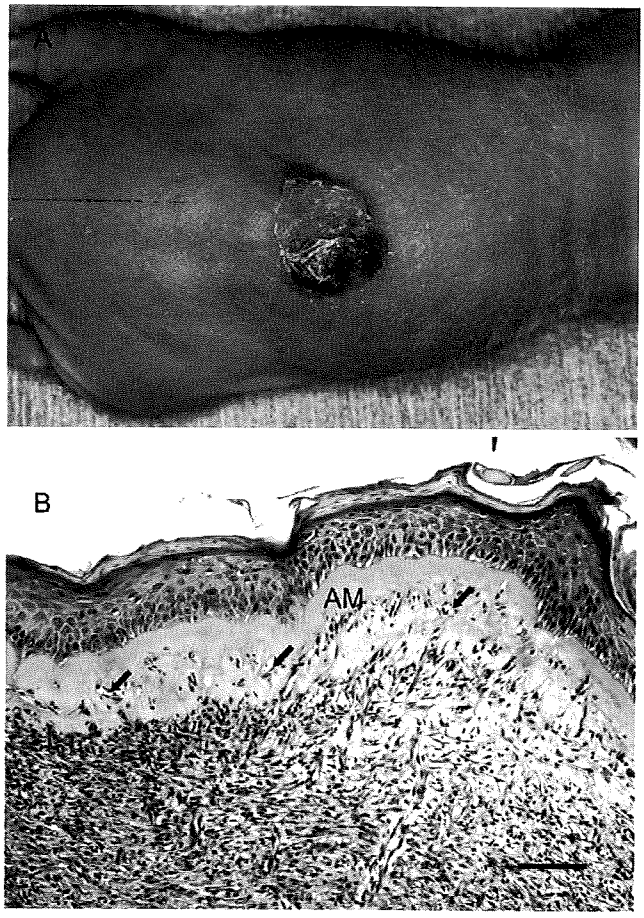

Fig. 6. Morphology of the living skin equivalent grafts. The living skin equivalents (LSEs) were grafted onto full-thickness wounds on the backs of nude mice. Two weeks later, the gross appearance of the grafts was photographed and the grafts were harvested and processed for H&E staining. A well stratified and differentiated epidermis was observed. Many small blood vessels were found in the substratum of the graft (arrows) up to near the thin acellular zone, which separated the epidermis and underlying substratum. AM, amnion. Bar is 50 μm.

The FASEB Journal article fj.09-145292. Published online December 29, 2009.
The FASEB Journal • Research Communication

Identification of novel hair-growth inducers by means of connectivity mapping

Yumiko Ishimatsu-Tsuji, Tsutomu Soma, and Jiro Kishimoto[1]
Shiseido Innovative Science Research and Development Center, Yokohama, Japan

ABSTRACT **The aim of this study was to identify novel inducers of hair growth using gene expression profiling at various stages of hair-growth induction. First, we analyzed gene expression at the onset of hair growth in mice induced by cyclosporin A (CsA), a well-known hair-growth inducer, using DNA microarray analysis. The results unveiled genes involved in the step-by-step progression of hair growth, including increases in melanin biosynthesis and decreases in immune response at d 2 and the subsequent stimulation of cell proliferation at d 4, followed by the up-regulation of hair specific keratins at d 7 after CsA treatment. With the use of the connectivity map (Cmap), agents that had a similar "gene signature" to that of the profiles of CsA-treated mice were identified. Several agents, including CsA, were identified by the Cmap and were evaluated for hair induction activity *in vivo*. One of the proposed agents, fluphenazine (from the d 2 signature) actually induced hair growth *in vivo* (ED_{50}: 2 mM for single application), and the subsequent application of 5 mM iloprost (from the d 4 signature) significantly enhanced the hair-growth effect of fluphenazine. From these results, Cmap analysis was proven to be a useful method that connects gene expression profiles of complicated biological processes, such as hair-growth induction, to effective agents.—Ishimatsu-Tsuji, Y., Soma, T., Kishimoto, J. Identification of novel hair-growth inducers by means of connectivity mapping. *FASEB J.* 24, 000–000 (2010). www.fasebj.org**

Key Words: Cmap · microarray · hair follicle · cyclosporin · fluphenazine · iloprost

THE HAIR FOLLICLE IS A VERY characteristic miniorgan, which cyclically grows, regresses, and detaches, after which new hairs grow. The hair cycle is staged into 3 phases: anagen (the growing phase), catagen (the regressing phase), and telogen (the resting phase; refs. 1, 2). Aberrations of the hair cycle are known to cause hair loss or unwanted hair growth (3), and elucidating the biology and pathology of the hair cycle should lead to effective therapies for disorders of the hair cycle. Multiple regulators of the hair cycle have been identified, such as growth factors, adhesion molecules, cytokines, hormones, neuropeptides, and transcription factors (reviewed in ref. 4) and multiple gene expression profiling studies have been reported (5–7). However, it has been difficult to connect the numerous factors identified to agents that are active in controlling the hair cycle *in vivo*. One of the underlying causes may be that the hair cycle proceeds in a stepwise fashion and is regulated cooperatively and synchronously by numerous factors.

In 2006, an innovative method, named the "connectivity map" (Cmap), was reported by Lamb *et al.* (8) and commented on by Michnick (9). The investigators created a large public database containing hundreds of gene expression profiles, called "reference gene signatures," of cultured human cells treated with >100 bioactive small molecules, attached to a pattern-matching tool. Researchers can access that database *via* the Internet and can compare gene signatures of interest with the Cmap database. The pattern-matching software scores and ranks similarities between the researcher's and the reference signatures and can lead to unexpected connections between the researcher's gene profiling data and small molecules. With the use of that method, novel agents were identified that could solve the problem of anticancer drug resistance, and novel inhibitory mechanisms of androgen receptor inhibitors were reported (10, 11). More recently, several studies (12–18), mainly on cancer research, reported the use of this method.

In this study, to identify novel trichogenous agents using the Cmap method, we initially performed gene expression profiling on the dorsal skin of mice in which hair growth was induced by the topical application of cyclosporin A (CsA), a well-known potent hair-growth inducer. The gene signatures of the CsA-treated mice were then queried in the Cmap database. Agents that were highly ranked in Cmap were topically applied on the dorsal skin of mice to determine whether they induce hair growth like CsA.

MATERIALS AND METHODS

Anagen induction by topical application of CsA

Anagen was induced essentially as described previously (19). Female 8-wk-old C3H/HeJ mice whose hair cycle was at

[1] Correspondence: Shiseido Innovative Science Research and Development Center, 2-12-1, Fukuura, Kanazawa-ku, Yokohama, Kanagawa 236-8643, Japan. E-mail: jiro.kishimoto@to.shiseido.co.jp
doi: 10.1096/fj.09-145292

0892-6638/10/0024-0001 © FASEB

telogen were purchased from Hoshino Laboratory Animals (Saitama, Japan). Their dorsal hair was carefully cut with animal hair clippers, followed by a single topical application of 100 μl of 10 mM CsA in 95% ethanol or 100 μl vehicle as a control on the dorsal skin. This study was approved by the ethics committee of our institute in accordance with the guidelines of the National Institutes of Health.

Microarray analysis

Total RNAs were extracted from the dorsal skin of mice at d 2, 4, and 7 after CsA treatment, as described previously (7). Double-stranded cDNAs were synthesized from the total RNAs, after which cyan 3- or 5-labeled cRNAs were made from the cDNAs using *in vitro* transcription according to the manufacturer's instructions (Agilent Technologies, Palo Alto, CA, USA). Labeled cRNAs were hybridized with 2-color oligo microarray chips [Whole Mouse Genome (44K); G4122F; Agilent Technologies]. After being washed, the fluorescence of each hybridized cRNA on the chip was quantified in a microarray scanner (Agilent Dual-Laser Microarray Scanner G2565AA). The scanned data were analyzed using Feature Extraction Software 9.1 (Agilent Technologies), which tagged the data as signals recognized as outliers or equal to the background. The fold change of each gene was calculated as the ratio of signal intensity between the experimental data and the control data. Two independent experiments were performed for each set of data comparing CsA *vs.* vehicle treatment. The microarray data were deposited in the Gene Expression Omnibus (GEO) database (accession no. GSE16739; http://www.ncbi.nlm.nih.gov/geo) and described in accordance with the Minimum Information About a Microarray Experiment (MIAME) guidelines.

Data processing of microarray analysis

For the bioinformatic analysis, the data were processed with Gene Spring GX 7.3.1 software (Agilent Technologies) according to the manufacturer's instructions. Data that were tagged as outliers or equal to the background in each chip were excluded, and genes that were reproducibly up- or down-regulated >1.5-fold at each time point after CsA treatment were listed. The significance of the enrichment of the Gene Ontology categories (http://www.geneontology.org) in each gene list was calculated statistically using Fisher's exact test.

Cmap analysis

The details of the Cmap database have been described by Lamb *et al.* (8). In this method, the similarity between each researcher's microarray results (the query signature) and 453 microarray results for ~164 agents (reference signatures) in the Cmap database was evaluated using the Kolmogorov-Smirnov statistic, a nonparametric, rank-based pattern-matching strategy. Each reference signature in the database was scored according to its similarity with the query signature, and the extent of the similarity is described as the "connectivity score." The connectivity score ranges from +1 to −1; nearer to +1 means higher similarity, 0 means no similarity, and nearer to −1 means opposite similarity. For the query, the probe ID defined by the Affymetrix GeneChip Human Genome U133A array (Affymetrix, Santa Clara, CA, USA) was used. Here, the probe ID of U133A corresponding to the signatures of d 2 and 4 after CsA treatment were identified using Gene Spring software (Supplemental Tables S5 and S6), followed by the query in the Cmap database *via* the Internet (http://www.broad.mit.edu/cmap). "Permutated results," which consist of the arithmetic means of the connectivity scores and the statistical significance of the replicates (calculated as "enrichment" and "permutation *P* value" at the Cmap), were used to evaluate the significance of the scores.

Hair-growth induction test

The hair-growth induction test was performed mostly as described above. Test samples were applied 1×/d for 1 d or for 30 sequential days. The level of hair growth was evaluated at 30 d after the start of the application using photograph image analysis; that is, mice with a trichogenous area of <70% were defined as "partial trichogenous," and those with >70% were defined as "wholly trichogenous." Supplemental Tables S8–S10 show the agents tested, the applied doses, and the duration of treatments. To test the combinatory effects of fluphenazine and prostacyclin (PGI) derivatives with a stepwise application, fluphenazine was first applied for 3 d, after which the PGI derivatives (iloprost, beraprost, epoprostenol, or treprostenil) were applied for 2 d. To test the mixed application of fluphenazine and iloprost, the agents were mixed and applied for 2 d.

Chemicals

Fluphenazine, topiramate, yohimbine, tetraethylenepentamine, (−)-catechin, prednisolone, clozapine, trifluoperazine, chlorpromazine, thioridazine, prochlorperazine, and quinpirole were purchased from Sigma-Aldrich Japan K.K. (Tokyo, Japan). Genistein, geldanamycin, and U0125 were purchased from Calbiochem (Darmstadt, Germany). Iloprost, beraprost, epoprostenol, and treprostenil were purchased from Cayman Chemical (Ann Arbor, MI, USA), and DL-PPMP was purchased from Biomol International (Plymouth Meeting, MA, USA).

RESULTS

Identification of gene signatures at the onset of hair growth induced by CsA

To induce hair growth, CsA was topically applied on the dorsal skin of 8-wk-old C3H mice, all hairs at that age being in telogen. The induced hairs emerged from the skin surface 11 d after the CsA treatment. **Figure 1** shows the morphological changes of pelage hair follicles sequentially after CsA treatment. In preliminary experiments (performed in triplicate), we determined that no genes were up- or down-regulated reproducibly at d 1; thus, we analyzed stages at 2 d and later after CsA treatment. At d 2, little or no morphological change was observed, and the hairs were classified into the stage between telogen and anagen I, according to the classification by Muller-Rover *et al.* (20). At d 4, thickening of keratinocyte strands between the dermal papilla (DP) and club hairs was observed; these were classified as anagen I and II hairs. At d 7, anagen IIIa–IIIc hairs were mainly observed with newly formed hair shafts and melanin above the DP. Meanwhile, in control mice treated with vehicle, all hairs remained in telogen from d 2 through 7. From these observations, the hair cycle induction was thought to be initiated within 4 d after CsA treatment.

keratinocytes attached and spread faster on de-epithelialized AM and that confluent cells were more compactly arranged than on type I collagen. Also, in a previous study, we showed that newly formed epidermis expanded faster on de-epithelialized amnions than on fibroblast-populated type I collagen gel [32]. Among the main BM components, type IV collagen has been shown to enhance human keratinocyte spread and growth [36], and laminin 5, a key component of the anchoring complex of the BM, is also essential for keratinocyte attachment, polarization, and migration [37–39].

When constructing a LSE, preexisting BM components on the dermal matrix contribute to improving the morphology of the epidermis and are necessary for the formation of hemidesmosomes and the development of a lamina densa [9,40,41]. Epithelial–mesenchymal interactions play important roles in controlling epidermal morphogenesis and homeostasis. The interaction between keratinocytes and the insoluble BM proteins contributes to the maintenance of tissue architecture and affects various biological processes, such as cell attachment, proliferation, differentiation, and migration [42,43]. On the de-epithelialized AM, the epidermis was well differentiated, stratified, and polarized, with columnar basal cells compactly aligned along the dermal–epidermal junction. These results indicated that the presence of certain BM components on de-epithelialized AM improved the homeostasis of the overlying epidermis.

The well developed basal lamina and hemidesmosomes in the amnion LSE guaranteed a stable association between the epidermis and the underlying tissues, which could explain why the epidermis was resistant to separation from the underlying connective tissue when the LSEs were harvested and manipulated for grafting.

Fibroblasts support epidermal morphogenesis and the deposition of BM components in preparing a LSE [44,45]. We constructed a LSE by seeding keratinocytes on de-epithelialized amnions; however, without coculturing fibroblasts in the stroma of the amnions, the resulting epidermis was thin and the basal cells were not well organized (data not shown). Because fibroblasts are known to support the growth of monolayer keratinocytes, we prepared fibroblasts in six-well plates to nourish the keratinocytes, which were seeded onto de-epithelialized amnions in culture inserts (set in six-well plates), and cultivated the keratinocytes at the air–liquid interface. However, the resulting epidermis of the LSEs was only two to three layers thick, and the cells were disorganized on the amnions (data not shown). It appears that fibroblasts being cultivated in the dermal matrix and the formation of a three-dimensional network are important for a well organized and differentiated epidermis in a LSE.

In the transplantation experiment, amnion LSEs were readily harvested from the culture inserts and transferred to full-thickness wounds on the backs of nude mice. The LSE grafts survived well on the nude mice and were well vascularized, as seen in the H&E-stained sections.

We also confirmed some other advantages in making the amnion LSE. First, we did not use any animal-derived type I collagen gel, which is conventionally employed in constructing the dermal matrix for a LSE [33]. Type I collagen is costly and may cause inflammatory reactions upon transplantation, and ethical issues may arise because of its animal origin [46]. Second, the procedure is simpler in making a fibroblast-infiltrated amnion than a fibroblast-populated collagen gel, which requires the mixing of several different ingredients while stirring on ice. Third, amnions as the matrix are more resistant to shear forces than collagen gel, which greatly facilitates the manipulation in removing the LSE from the culture insert and transferring it to a wound bed in transplantation.

In conclusion, the LSE with amnions as the dermal matrix demonstrated various advantages, such as a simple cultivating procedure, low cost, good mechanical and handling properties, and containing no animal products. Good epidermogenesis was seen *in vivo* and *in vitro*, suggesting that this LSE may be useful for clinical applications.

Acknowledgments

We thank Keiko Ozaki, Teruko Tsuda, and Eriko Tan for their technical assistance. This work was supported in part by grants from the Ministries of Education, Culture, Sports, Science and Technology, Japan, and in part by Health and Labor Sciences Research Grants (Research on Intractable Diseases) from the Ministry of Health, Labour and Welfare of Japan.

References

[1] Waymack P, Duff RG, Sabolinski M. The effect of a tissue engineered bilayered living skin analog, over meshed split-thickness autografts on the healing of excised burn wounds. The Apligraf Burn Study Group. Burns 2000;26:609–19.
[2] Falanga V, Margolis D, Alvarez O, Auletta M, Maggiacomo F, Altman M, et al. Rapid healing of venous ulcers and lack of clinical rejection with an allogeneic cultured human skin equivalent. Human Skin Equivalent Investigators Group. Arch Dermatol 1998;134:293–300.
[3] Kirsner RS. The use of Apligraf in acute wounds. J Dermatol 1998;25:805–11.
[4] Andriani F, Margulis A, Lin N, Griffey S, Garlick JA. Analysis of microenvironmental factors contributing to basement membrane assembly and normalized epidermal phenotype. J Invest Dermatol 2003;120:923–31.
[5] Jean J, Lapointe M, Soucy J, Pouliot R. Development of an in vitro psoriatic skin model by tissue engineering. J Dermatol Sci 2009;53:19–25.
[6] Wang X, Liu Y, Deng Z, Dong R, Liu Y, Hu S, et al. Inhibition of dermal fibrosis in self-assembled skin equivalents by undifferentiated keratinocytes. J Dermatol Sci 2009;53:103–11.
[7] Meana A, Iglesias J, Del Rio M, Larcher F, Madrigal B, Fresno MF, et al. Large surface of cultured human epithelium obtained on a dermal matrix based on live fibroblast-containing fibrin gels. Burns 1998;24:621–30.
[8] Llames SG, Del Rio M, Larcher F, Garcia E, Garcia M, Escamez MJ, et al. Human plasma as a dermal scaffold for the generation of a completely autologous bioengineered skin. Transplantation 2004;77:350–5.
[9] Medalie DA, Eming SA, Collins ME, Tompkins RG, Yarmush ML, Morgan JR. Differences in dermal analogs influence subsequent pigmentation, epidermal differentiation, basement membrane, and rete ridge formation of transplanted composite skin grafts. Transplantation 1997;64:454–65.
[10] Guerret S, Govignon E, Hartmann DJ, Ronfard V. Long-term remodeling of a bilayered living human skin equivalent (Apligraf) grafted onto nude mice: immunolocalization of human cells and characterization of extracellular matrix. Wound Repair Regen 2003;11:35–45.
[11] Ojeh NO, Frame JD, Navsaria HA. In vitro characterization of an artificial dermal scaffold. Tissue Eng 2001;7:457–72.
[12] Morykwas MJ, Thornton JW, Bartlett RH. Zeta potential of synthetic and biological skin substitutes: effects on initial adherence. Plast Reconstr Surg 1987;79:732–9.
[13] Ravishanker R, Bath AS, Roy R. "Amnion Bank"—the use of long term glycerol preserved amniotic membranes in the management of superficial and superficial partial thickness burns. Burns 2003;29:369–74.
[14] Gajiwala K, Gajiwala AL. Evaluation of lyophilised, gamma-irradiated amnion as a biological dressing. Cell Tissue Bank 2004;5:73–80.
[15] Quinby Jr WC, Hoover HC, Scheflan M, Walters PT, Slavin SA, Bondoc CC. Clinical trials of amniotic membranes in burn wound care. Plast Reconstr Surg 1982;70:711–7.
[16] Park M, Kim S, Kim IS, Son D. Healing of a porcine burn wound dressed with human and bovine amniotic membranes. Wound Repair Regen 2008;16:520–8.
[17] Mohammadi A, Johari HG. Amniotic membrane: a skin graft fixator convenient for both patient and surgeon. Burns 2008;34:1051–2.
[18] Oyama N, Bhogal BS, Carrington P, Gratian MJ, Black MM. Human placental amnion is a novel substrate for detecting autoantibodies in autoimmune bullous diseases by immunoblotting. Br J Dermatol 2003;148:939–44.
[19] Koizumi N, Fullwood NJ, Bairaktaris G, Inatomi T, Kinoshita S, Quantock AJ. Cultivation of corneal epithelial cells on intact and denuded human amniotic membrane. Invest Ophthalmol Vis Sci 2000;41:2506–13.
[20] Nakamura T, Endo K, Cooper LJ, Fullwood NJ, Tanifuji N, Tsuzuki M, et al. The successful culture and autologous transplantation of rabbit oral mucosal epithelial cells on amniotic membrane. Invest Ophthalmol Vis Sci 2003;44:106–16.
[21] Sakamoto T, Hirano K, Morishima Y, Masuyama K, Ishii Y, Nomura A, et al. Maintenance of the differentiated type II cell characteristics by culture on an acellular human amnion membrane. In Vitro Cell Dev Biol Anim 2001;37:471–9.
[22] Espana EM, He H, Kawakita T, Di Pascuale MA, Raju VK, Liu CY, et al. Human keratocytes cultured on amniotic membrane stroma preserve morphology and express keratocan. Invest Ophthalmol Vis Sci 2003;44:5136–41.

[23] Kumar TR, Shanmugasundaram N, Babu M. Biocompatible collagen scaffolds from a human amniotic membrane: physicochemical and in vitro culture characteristics. J Biomater Sci Polym Ed 2003;14:689–706.
[24] Kubo M, Sonoda Y, Muramatsu R, Usui M. Immunogenicity of human amniotic membrane in experimental xenotransplantation. Invest Ophthalmol Vis Sci 2001;42:1539–46.
[25] Solomon A, Wajngarten M, Alviano F, Anteby I, Elchalal U, Pe'er J, et al. Suppression of inflammatory and fibrotic responses in allergic inflammation by the amniotic membrane stromal matrix. Clin Exp Allergy 2005;35:941–8.
[26] Burman S, Tejwani S, Vemuganti GK, Gopinathan U, Sangwan VS. Ophthalmic applications of preserved human amniotic membrane: a review of current indications. Cell Tissue Bank 2004;5:161–75.
[27] von Versen-Hoynck F, Syring C, Bachmann S, Moller DE. The influence of different preservation and sterilisation steps on the histological properties of amnion allografts—light and scanning electron microscopic studies. Cell Tissue Bank 2004;5:45–56.
[28] Rejzek A, Weyer F, Eichberger R, Gebhart W. Physical changes of amniotic membranes through glycerolization for the use as an epidermal substitute. Light and electron microscopic studies. Cell Tissue Bank 2001;2:95–102.
[29] von Versen-Hoeynck F, Steinfeld AP, Becker J, Hermel M, Rath W, Hesselbarth U. Sterilization and preservation influence the biophysical properties of human amnion grafts. Biologicals 2008;36:248–55.
[30] Shirakata Y, Ueno H, Hanakawa Y, Kameda K, Yamasaki K, Tokumaru S, et al. TGF-beta is not involved in early phase growth inhibition of keratinocytes by 1alpha,25(OH)2vitamin D3. J Dermatol Sci 2004;36:41–50.
[31] Shirakata Y, Tokumaru S, Yamasaki K, Sayama K, Hashimoto K. So-called biological dressing effects of cultured epidermal sheets are mediated by the production of EGF family, TGF-beta and VEGF. J Dermatol Sci 2003;32:209–15.
[32] Yang L, Shirakata Y, Shudou M, Dai X, Tokumaru S, Hirakawa S, et al. New skin-equivalent model from de-epithelialized amnion membrane. Cell Tissue Res 2006;326:69–77.
[33] Yang L, Shirakata Y, Tamai K, Dai X, Hanakawa Y, Tokumaru S, et al. Microbubble-enhanced ultrasound for gene transfer into living skin equivalents. J Dermatol Sci 2005;40:105–14.
[34] Cooper LJ, Kinoshita S, German M, Koizumi N, Nakamura T, Fullwood NJ. An investigation into the composition of amniotic membrane used for ocular surface reconstruction. Cornea 2005;24:722–9.
[35] Nakamura T, Yoshitani M, Rigby H, Fullwood NJ, Ito W, Inatomi T, et al. Sterilized, freeze-dried amniotic membrane: a useful substrate for ocular surface reconstruction. Invest Ophthalmol Vis Sci 2004;45:93–9.
[36] Woodley DT, Wynn KC, O'Keefe EJ. Type IV collagen and fibronectin enhance human keratinocyte thymidine incorporation and spreading in the absence of soluble growth factors. J Invest Dermatol 1990;94:139–43.
[37] Nishiyama T, Amano S, Tsunenaga M, Kadoya K, Takeda A, Adachi E, et al. The importance of laminin 5 in the dermal-epidermal basement membrane. J Dermatol Sci 2000;24:S51–9.
[38] Frank DE, Carter WG. Laminin 5 deposition regulates keratinocyte polarization and persistent migration. J Cell Sci 2004;117:1351–63 [Epub 2004 Mar 1302].
[39] Kikkawa Y, Umeda M, Miyazaki K. Marked stimulation of cell adhesion and motility by ladsin, a laminin-like scatter factor. J Biochem (Tokyo) 1994;116:862–9.
[40] Kim SW, Park KC, Kim HJ, Cho KH, Chung JH, Kim KH, et al. Effects of collagen IV and laminin on the reconstruction of human oral mucosa. J Biomed Mater Res 2001;58:108–12.
[41] Ralston DR, Layton C, Dalley AJ, Boyce SG, Freedlander E, Mac Neil S. The requirement for basement membrane antigens in the production of human epidermal/dermal composites in vitro. Br J Dermatol 1999;140:605–15.
[42] Blomme EA, Weckmann MT, Capen CC, Rosol TJ. Influence of extracellular matrix macromolecules on normal human keratinocyte phenotype and parathyroid hormone-related protein secretion and expression in vitro. Exp Cell Res 1998;238:204–15.
[43] Kim JP, Chen JD, Wilke MS, Schall TJ, Woodley DT. Human keratinocyte migration on type IV collagen. Roles of heparin-binding site and alpha 2 beta 1 integrin. Lab Invest 1994;71:401–8.
[44] Erdag G, Sheridan RL. Fibroblasts improve performance of cultured composite skin substitutes on athymic mice. Burns 2004;30:322–8.
[45] El Ghalbzouri A, Ponec M. Diffusible factors released by fibroblasts support epidermal morphogenesis and deposition of basement membrane components. Wound Repair Regen 2004;12:359–67.
[46] Klein B, Schiffer R, Hafemann B, Klosterhalfen B, Zwadlo-Klarwasser G. Inflammatory response to a porcine membrane composed of fibrous collagen and elastin as dermal substitute. J Mater Sci Mater Med 2001;12:419–24.

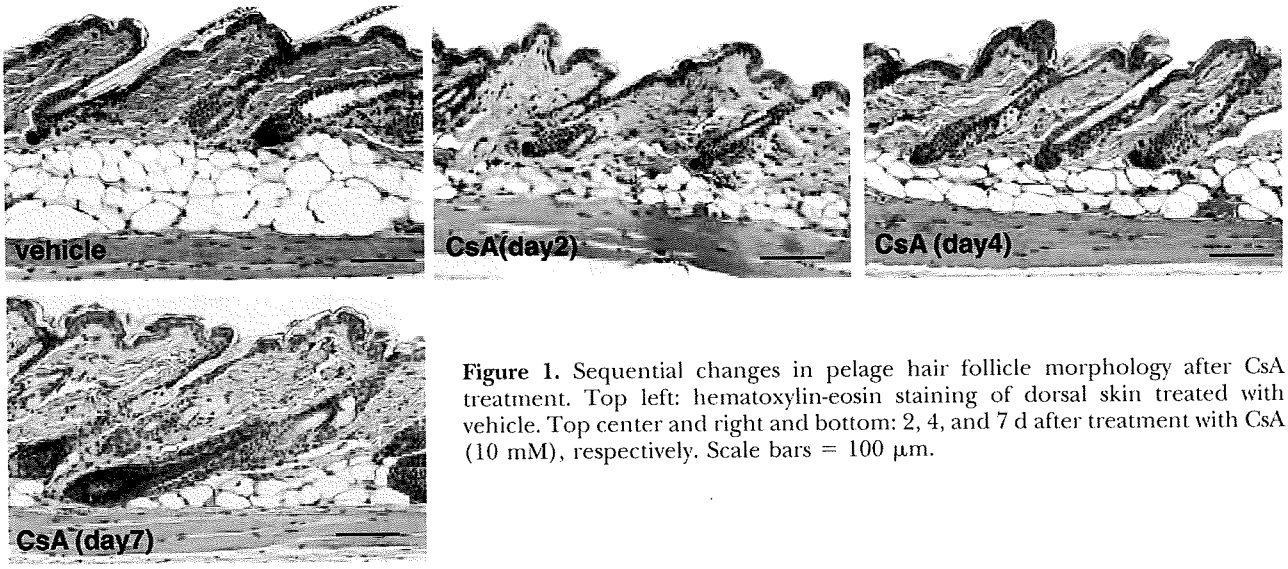

Figure 1. Sequential changes in pelage hair follicle morphology after CsA treatment. Top left: hematoxylin-eosin staining of dorsal skin treated with vehicle. Top center and right and bottom: 2, 4, and 7 d after treatment with CsA (10 mM), respectively. Scale bars = 100 μm.

The gene expression profiles at d 2, 4, and 7 after CsA treatment compared with vehicle-treated controls were examined by DNA microarray analysis. Genes that reproducibly up- or down-regulated >1.5-fold at each time point in duplicate microarrays are listed (**Fig. 2** and Supplemental Tables S1–S3). The number of genes whose expression was changed increased day by day after CsA treatment. The functional groups and biological relevance of the listed genes are shown in **Table 1** and in Supplemental Table S4. The increased expression of genes involved in melanin biosynthesis and the down-regulation of genes involved in immune responses occurred at d 2, when the onset stage of hair growth occurs, and persisted at d 4 and 7. At d 4, cell division occurs actively as supported by the expression pattern of genes involved in that process. At d 7, multiple structural proteins more specific to the hair follicle than at d 4, *e.g.*, hair keratins in the category of "cytoskeleton organization and biosynthesis," were up-regulated, suggesting the start of the structural formation of the hair follicle.

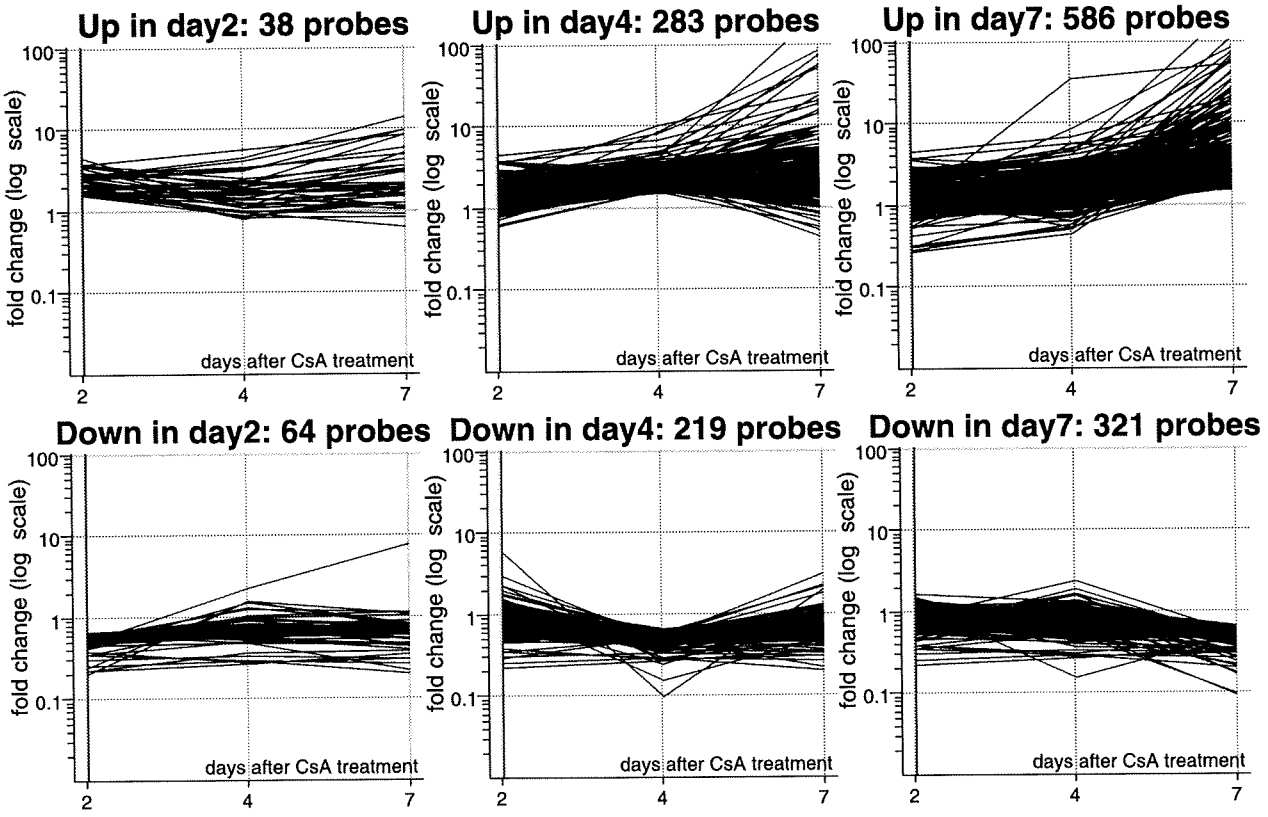

Figure 2. Overview of the expression patterns of genes up- or down-regulated at 2, 4, and 7 d after CsA treatment.

TABLE 1. *Gene ontology categories that have overlap with the list of the up- or down-regulated genes*

Category	Genes in category[a]		Genes in list in category[b]		
	n	%	*n*	%	*P* value[c]
Up-regulated					
Day 2					
GO:42438: melanin biosynthesis	12	0.051	2	10.0	4.52E-05
GO:42438: melanin biosynthesis	12	0.051	4	2.0	2.29E-06
Day 4					
GO:51301: cell division	432	1.838	38	19.2	1.21E-27
GO:7010: cytoskeleton organization and biogenesis	966	4.109	16	8.1	7.88E-03
GO:42438: melanin biosynthesis	12	0.051	5	1.2	1.33E-06
Day 7					
GO:51301: cell division	432	1.838	47	11.1	3.68E-23
GO:7010: cytoskeleton organization and biogenesis	966	4.109	40	9.4	1.02E-06
GO:6633: fatty acid biosynthesis	106	0.451	8	1.9	6.78E-04
Down-regulated					
Day 2					
GO:6955: immune response	1022	4.347	9	22.5	4.33E-05
Day 4					
GO:6955: immune response	1022	4.347	36	20.69	4.09E-15
Day 7					
GO:6955: immune response	1022	4.347	45	18.15	2.90E-16
GO:6936: muscle contraction	139	0.591	9	3.629	1.74E-05

[a]Total number of genes on the chip that have been assigned to the category, and percentage of genes assigned to this category per total number of all genes nominated in GO. [b]Total number of genes that are both in the list of the up- or down-regulated genes and in the category, and percentage of genes that fall into this category per total number of annotated genes in the list of up- or down-regulated genes. [c]Statistical significance of the overlap, *i.e.*, likelihood that it is a coincidence that these genes were in both the list of the up- or down-regulated genes and the category.

Cmap analysis connects the gene signature of CsA-treated mice to CsA and to the novel trichogenous agent fluphenazine

To identify agents that could induce hair growth like CsA, the signatures derived from the onset of hair growth, at d 2 and 4 after CsA treatment, were queried in the Cmap database. As a result, 96 and 62 of 453 reference signatures were positively scored with the d 2 and d 4 signatures, respectively (Supplemental Table S7). It is noteworthy that both replicates of the CsA reference signatures were positively scored in the Cmap of d 2.

Since the profiling data derived from the CsA-treated skin identified the same compound by the Cmap, other positively scored agents could also have effects like CsA. Thirteen agents that were highly ranked or were reproducibly and positively scored in the Cmap were selected as putative CsA-like agents (**Table 2**). In detail, we mainly relied on the permutated result (Supplemental Table S7) in the Cmap to identify significantly highly scored agents among the positively scored agents. First, with the d 2 signature, agents that were more highly ranked than CsA in the permutated results and where more than half the replicates were scored positively were selected. Thus, fluphenazine, geldanamycin, and clozapine were selected. Tetraethylenepentamine was also selected because it was positively scored reproducibly with both the d 2 and d 4 signatures. With the d 4 signature, agents more highly ranked than tetraethylenepentamine in the permutated results were selected, *i.e.*, iloprost and genistein. Agents without replicates were selected considering their availabilities. To evaluate the possible trichogenous effects of these 13 selected agents, they were topically applied on mouse dorsal skin and hair-growth induction tests were performed. Fluphenazine, a D2 dopaminergic receptor antagonist, significantly induced hair growth (Supplemental Table S8). Because no apparent skin irritation (characterized by redness, dryness, or flaking), which can itself induce hair growth, was observed, that was not the cause of the fluphenazine-induced hair growth. The ratio of mice with induced hair growth of all surviving mice that were tested depended on the dose of fluphenazine used, either for 1 or for 30 d (**Fig. 3*A***). Even though fluphenazine induced hair growth in some of the tested mice, we could not apply sufficient doses to induce hair growth in all mice, because the dose of fluphenazine that can be used is limited by its toxicity (Fig. 3*A* and Supplemental Table S8). No trichogenous effects were observed with the 4 phenothiazine derivatives tested that are analogous to fluphenazine (trifluoperazine, chlorpromazine, thioridazine, and prochlorperazine).

Hair-growth effect of fluphenazine is enhanced by the subsequent application of iloprost

Considering the step-by-step progression of the onset of the hair growth, the additive effects of agents proposed by the Cmap analysis at different time points was expected. Thus, we tested the combinatorial effect of

TABLE 2. *Agents highly ranked in the Cmap*

Agent	*n*	Connectivity score/dose/cell
Day 2 signature		
Yohimbine	1	0.909/23 μM/MCF7
Clozapine	2	0.83/10 μM/MCF7, 0.641/10 μM/MCF7
Topiramate	1	0.727/3 μM/MCF7
Fluphenazine	4	0.977/10 μM/MCF7, 0.861/10 μM/MCF7, 0.589/10 μM/SKM EL5, 0.0/10 μM/MCF7
Geldanamycin	6	0.82/1 μM/MCF7, 0.646/1 μM/MCF7, 0.646/1 μM/MCF7, 0.552/1 μM/MCF7, 0.504/1 M/MCF7, 0.0/1 μM/MCF7
Cyclosporin A	2	0.521/1 μM/MCF7, 0.425/1 μM/MCF7
Tetraethylenepentamine	6	0.666/100 μM/ssMCF7, 0.557/100 μM/PC3, 0.55/100 μM/MCF7, 0.52 1/10 μM/MCF7, 0.0/100 μM/HL60, 0.0/100 μM/MCF7
Day 4 signature		
U0125	1	0.941/1 μM/PC3
Iloprost	3	0.918/1 μM/MCF7, 0.87 1/1 μM/M CF7, 0.745/1 μM/SKM EL5
DL-PPM P	1	0.831/2 μM/MCF7
(−)-Catechin	1	0.78/11 μM/MCF7
Prednisolone	1	0.725/1 μM/MCF7
Yohimbine	1	0.71/23 μM/MCF7
Quinpirole	1	0.584/1 μM/MCF7
Genistein	7	1.0/1 μM/MCF7, 0.804/10 μM/MCF7, 0.761/10 μM/MCF7, 0.757/1 μM/MCF7, 0.0/10 μM/MCF7, 0.0/10 μM/PC 3, −0.604/10 μM/MCF7
Tetraethylenepentamine	6	0.694/100 μM/PC3, 0.678/100 μM/MCF7, 0.565/100 μM/HL60, 0.0/10 μM/MCF7, 0.0/100 μM/ssMCF7, 0.0/100 μM/MCF7

Dose, concentration of bioactive small molecules used in the reference signature; cell, cell lines used in the reference signature.

fluphenazine (from the d 2 signature of CsA-induced hair growth) with iloprost, a prostaglandin I analog (which was highly ranked in the Cmap of the d 4 signature). We chose iloprost from the list of 9 agents (d 4 signature) for combinatorial treatment because its rank in the permutated results was the highest. Fluphenazine was applied first for 3 d, and then iloprost, which is supposed to induce similar phenomena at d 4 of CsA-induced hair growth, was applied starting at 4 d after the start of fluphenazine treatment for another 2 d. As a result, a markedly higher ratio of mice treated with fluphenazine and iloprost showed hair growth compared with the application of fluphenazine only (Fig. 3*B* and Supplemental Table S9). No hair growth was observed in vehicle-treated or in iloprost-only treated mice (Fig. 3*C, D*). The speed of induced hair growth was indistinguishable between the single application of fluphenazine and the sequential application of fluphenazine and iloprost (Fig. 3*E, F*). Beraprost, an analog of prostaglandin I, also enhanced fluphenazine-induced hair growth but to a lesser extent (Fig. 3*B*). The enhancement of hair growth was not observed following the sequential treatment with 1 mM CsA and iloprost. Moreover, the hair-growth effect of fluphenazine was not enhanced by treatment with fluphenazine and iloprost together (Supplemental Table S10). This suggests that iloprost does not act to initiate hair growth by itself but potently enhances the hair growth induced by fluphenazine.

DISCUSSION

In this study, we analyzed the gene expression profiles at the onset of hair growth induced by CsA and unveiled sequential changes in gene expression during the hair-growth cycle. Taking advantage of the Cmap, the gene signature at d 2 after CsA treatment identified a functional analog of CsA, fluphenazine, that could induce anagen in mice. Moreover, we showed the additive effect of fluphenazine and iloprost, the latter being highly ranked in the Cmap analysis at a later time point (d 4).

With the gene expression profiling at the onset of hair growth, note that silver and tyrosinase-related protein 1, which are related to melanogenesis, were up-regulated at a very early stage of anagen onset, far before the appearance of visible melanin granules or pigmented hair shafts (Supplemental Table S4). The other distinctive gene groups that changed in expression were related to the cell cycle at d 4 and to the hair shaft at d 7 and were consistent with the morphological changes during the hair-growth progression. On the other hand, the down-regulation of immune defense response-related genes could have resulted from the well-known immunosuppressive effect of CsA.

The Cmap is an innovative method developed in 2006 that was aimed to further analyze microarray analyses to identify related bioactive agents. With the use of that method, the recovery of dexamethasone resistance in MCL-1 by sirolimus and the inhibitory effect on HSP90 by celastrol and gedunin were discovered in 2006 (10, 11). In addition, a number of groups reported the effective use of the Cmap in 2008 (12–18). As was suggested, the Cmap database has been shown to be efficient in analyzing various kinds of phenomena, and we demonstrate the efficacy of the Cmap despite great differences in the experimental sources, mouse *vs.* human and dorsal skin *vs.* cultured cells, between

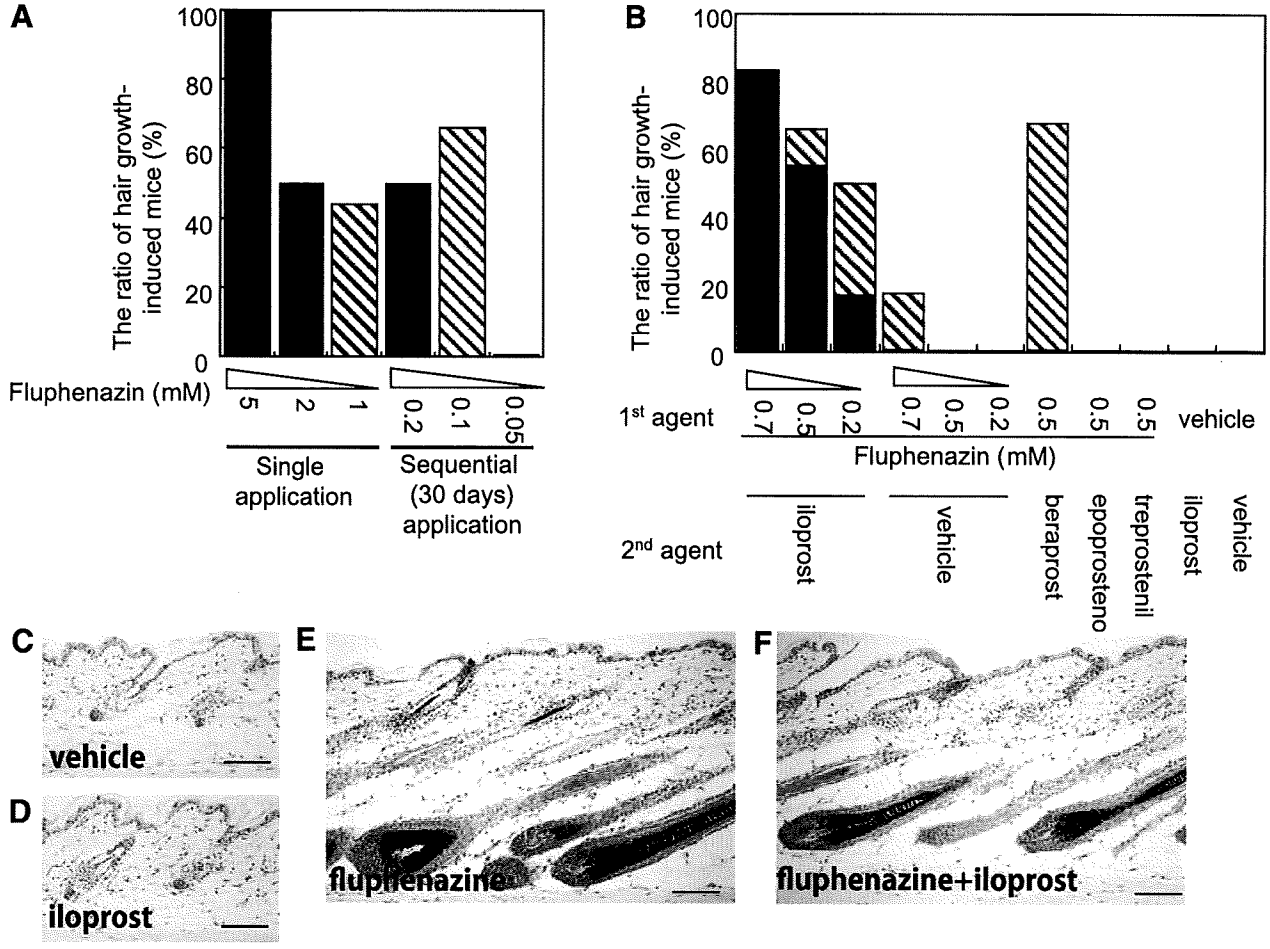

Figure 3. Effects of fluphenazine and iloprost on hair growth. *A*) Fluphenazine was topically applied on the dorsal skin of C3H mice once at a dose of 5, 2, or 1 mM, or for 30 sequential days at a dose of 0.2, 0.1, or 0.05 mM. *B*) Fluphenazine was topically applied at a dose of 0.7, 0.5, or 0.2 mM for the first 3 d followed by 5 mM iloprost, or by the PGI derivatives (beraprost, epoprostenol, and treprostenil), or by vehicle for 2 d. *A, B*) Ratio of number of mice with induced hair per total number of surviving mice tested from each group (n=3–9) was evaluated at 30 d after the first fluphenazine application. Solid columns, mice with induced hair on entire area of dorsal skin; striped columns, mice with induced hair on partial area (<70%) of dorsal skin. *C, D*) Hematoxylin-eosin staining of dorsal skin of representative mice at d 15 after the start of treatment with vehicle for 5 d (*C*) or 5 mM iloprost for 2 d (*D*). *E, F*) Hematoxylin-eosin staining of hair-induced areas of dorsal skin in mice with induced hair at d 15 after the start of the application with 0.7 mM fluphenazine for 3 d followed by 5 mM iloprost for 2 d (*E*) or 0.7 mM fluphenazine for 3 d followed by iloprost 5 mM for 2 d (*F*). Scale bars = 50 μm.

the query signature and the reference profiles. It is noteworthy that the combination of the large database and statistical tools could successfully connect CsA treatments in the Cmap with our d 2 signature despite differences, such as the species, which might reduce the similarity between them. These observations strongly suggest the robustness of the Cmap database analysis. However, the Cmap could have some weak points; for example, it should be affected by the experimental source to some extent, especially with sources more distant from human cells. Further, the accuracy and suitability of the signature are also important and the spectrum or limitation of agents included in the Cmap database might have an effect on the results.

The Cmap database was expanded after our analysis was performed. Therefore, we tested our signatures in the new version of the Cmap and found possible new candidates for hair growth (Supplemental Table S11). The agents for which the ratio of non-null permutated results were >50% and for which replicates were positively scored were considered to be significant. As a result, 412 agents for the d 2 signature and 380 agents for the d 4 signature were considered to be putative hair-growth inducers. The significance of the connection between the 4-d signature and iloprost is greatly enhanced in the new version of the Cmap. Thus, the second version of the Cmap is considered to be a powerful chemical genetic tool. On the other hand, the ranks of the permutated results of CsA (cyclosporin in the Cmap database) and fluphenazine were lower than in the first version. Although the scores of the same batches of the second version as that of first version of the Cmap were kept at the same level, the newly added batch with different doses, cell lines, or even the same experimental conditions that might have some small experimental differences from the first version (especially in the case of fluphenazine) reduced the significance of the connection. While the expanded version

of the Cmap is supposed to be a more reliable connection owing to the increased replicates and agents, there seem to be some cases that are more suitable for analysis with the first version due to the compatibility of the detailed experimental conditions of the database with that of the user. The dependency on the database limits the ability of the Cmap to some extent, even though the statistical tools and the large database diminish the limitations. The validation of the database might be useful for each user of the Cmap.

The search for complex phenomena, such as hair growth, could benefit from the Cmap owing to several points. First, hair-growth initiation is regulated by numerous factors in a orchestrated manner, so it is difficult to develop an effective hair-growth agent by screening enhancers or inhibitors of one protein, but the Cmap does not focus on each gene and avoids that complexity. Second, hair growth proceeds in a stepwise fashion. With the use of the Cmap, agents affecting each step could be identified from the gene signature of each step and the sequential application of agents is a powerful approach to synergize that phenomenon. One more point that is an advantage is that CsA, a potent hair-growth inducer, is included in the Cmap database. The fact that CsA itself could be connected to CsA-treated mice by the Cmap allowed us to evaluate the validity of the Cmap for our analysis.

Fluphenazine induces hair growth potently at doses similar to CsA. While fluphenazine is used as an antipsychotic drug and numerous side effects of oral administration have already been reported, such as extrapyramidal symptoms, sedation, and rash or edema of allergic dermatitis, the trichogenous effect elicited by its topical application was newly identified. The common functions of fluphenazine and CsA are suggestive about the mechanism of hair-growth induction. Fluphenazine is a phenothiazine derivative that antagonizes the dopamine D1/D2 receptor and inhibits calmodulin (21, 22). CsA has also been reported to induce hair growth *via* inhibition of the calcineurin-dependent activation of nuclear factor of activated T cells (NFAT; ref. 23). It is noteworthy that calcineurin is a calmodulin-dependent phosphatase. Therefore, it is possible that fluphenazine inhibits calmodulin, which might in turn inhibit calcineurin/NFAT and, following transcription, have a similar biological effect as CsA. Considering the recent report that the skin of mice in which calcineurin was disrupted showed cyclic alopecia (24) and that calcineurin/NFATc1 signaling governs the activity of hair follicle stem cells (25), this signaling pathway might be a good target for hair-growth induction. It also suggests that the 4 phenothiazine derivatives analogous to fluphenazine were not positively scored by the Cmap and that no trichogenous effects were observed. Fluphenazine is supposed to have some original characteristics, which could be a better percutaneous absorption or another effect distinct from its antagonism of the dopamine receptor and the inhibition of calmodulin.

Iloprost strongly enhanced the hair growth induced by fluphenazine, although it did not enhance hair growth by itself or with CsA. Beraprost also enhanced the hair-growth effect of fluphenazine but to a lesser extent. Iloprost and beraprost are structural analogues of PGI, which is clinically used as an agent to treat pulmonary hypertension (26). It is possible that vasodilation contributes to the effect or has some effect on cell proliferation, which is active at 4 d after CsA treatment. The stepwise (but not concomitant) application of iloprost enhanced the effect of fluphenazine, suggesting that it plays a role in a distinct stage after the hair growth is triggered by fluphenazine. The specific mechanism of iloprost remains unknown.

Taken together, our results demonstrate that the Cmap analysis is a useful postmicroarray analysis tool. In addition, this method can identify coeffective agents for physiological phenomena that proceed in a step-by-step fashion. FJ

REFERENCES

1. Hardy, M. H. (1992) The secret life of the hair follicle. *Trends Genet.* **8,** 55–61
2. Alonso, L., and Fuchs, E. (2006) The hair cycle. *J. Cell Sci.* **119,** 391–393
3. Paus, R., and Cotsarelis, G. (1999) The biology of hair follicles. *N. Engl. J. Med.* **341,** 491–497
4. Botchkarev, V. A., and Kishimoto, J. (2003) Molecular control of epithelial-mesenchymal interactions during hair follicle cycling. *J. Investig. Dermatol. Symp. Proc.* **8,** 46–55
5. Lin, K. K., Chudova, D., Hatfield, G. W., Smyth, P., and Andersen, B. (2004) Identification of hair cycle-associated genes from time-course gene expression profile data by using replicate variance. *Proc. Natl. Acad. Sci. U. S. A.* **101,** 15955–15960
6. Rendl, M., Lewis, L., and Fuchs, E. (2005) Molecular dissection of mesenchymal-epithelial interactions in the hair follicle. *PLoS Biol.* **3,** e331
7. Ishimatsu-Tsuji, Y., Moro, O., and Kishimoto, J. (2005) Expression profiling and cellular localization of genes associated with the hair cycle induced by wax depilation. *J. Invest. Dermatol.* **125,** 410–420
8. Lamb, J., Crawford, E. D., Peck, D., Modell, J. W., Blat, I. C., Wrobel, M. J., Lerner, J., Brunet, J. P., Subramanian, A., Ross, K. N., Reich, M., Hieronymus, H., Wei, G., Armstrong, S. A., Haggarty, S. J., Clemons, P. A., Wei, R., Carr, S. A., Lander, E. S., and Golub, T. R. (2006) The connectivity map: using gene-expression signatures to connect small molecules, genes, and disease. *Science* **313,** 1929–1935
9. Michnick, S. W. (2006) The connectivity map. *Nat. Chem. Biol.* **2,** 663–664
10. Wei, G., Twomey, D., Lamb, J., Schlis, K., Agarwal, J., Stam, R. W., Opferman, J. T., Sallan, S. E., den Boer, M. L., Pieters, R., Golub, T. R., and Armstrong, S. A. (2006) Gene expression-based chemical genomics identifies rapamycin as a modulator of MCL1 and glucocorticoid resistance. *Cancer Cell* **10,** 331–342
11. Hieronymus, H., Lamb, J., Ross, K. N., Peng, X. P., Clement, C., Rodina, A., Nieto, M., Du, J., Stegmaier, K., Raj, S. M., Maloney, K. N., Clardy, J., Hahn, W. C., Chiosis, G., and Golub, T. R. (2006) Gene expression signature-based chemical genomic prediction identifies a novel class of HSP90 pathway modulators. *Cancer Cell* **10,** 321–330
12. Setlur, S. R., Mertz, K. D., Hoshida, Y., Demichelis, F., Lupien, M., Perner, S., Sboner, A., Pawitan, Y., Andren, O., Johnson, L. A., Tang, J., Adami, H. O., Calza, S., Chinnaiyan, A. M., Rhodes, D., Tomlins, S., Fall, K., Mucci, L. A., Kantoff, P. W., Stampfer, M. J., Andersson, S. O., Varenhorst, E., Johansson, J. E., Brown, M., Golub, T. R., and Rubin, M. A. (2008) Estrogen-

dependent signaling in a molecularly distinct subclass of aggressive prostate cancer. *J. Natl. Cancer Inst.* **100,** 815–825
13. Garman, K. S., Acharya, C. R., Edelman, E., Grade, M., Gaedcke, J., Sud, S., Barry, W., Diehl, A. M., Provenzale, D., Ginsburg, G. S., Ghadimi, B. M., Ried, T., Nevins, J. R., Mukherjee, S., Hsu, D., and Potti, A. (2008) A genomic approach to colon cancer risk stratification yields biologic insights into therapeutic opportunities. *Proc. Natl. Acad. Sci. U. S. A.* **105,** 19432–19437
14. Hassane, D. C., Guzman, M. L., Corbett, C., Li, X., Abboud, R., Young, F., Liesveld, J. L., Carroll, M., and Jordan, C. T. (2008) Discovery of agents that eradicate leukemia stem cells using an in silico screen of public gene expression data. *Blood* **111,** 5654–5662
15. Zimmer, M., Ebert, B. L., Neil, C., Brenner, K., Papaioannou, I., Melas, A., Tolliday, N., Lamb, J., Pantopoulos, K., Golub, T., and Iliopoulos, O. (2008) Small-molecule inhibitors of HIF-2a translation link its 5′UTR iron-responsive element to oxygen sensing. *Mol. Cell* **32,** 838–848
16. Wang, S. E., Xiang, B., Guix, M., Olivares, M. G., Parker, J., Chung, C. H., Pandiella, A., and Arteaga, C. L. (2008) Transforming growth factor beta engages TACE and ErbB3 to activate phosphatidylinositol-3 kinase/Akt in ErbB2-overexpressing breast cancer and desensitizes cells to trastuzumab. *Mol. Cell. Biol.* **28,** 5605–5620
17. Rosenbluth, J. M., Mays, D. J., Pino, M. F., Tang, L. J., and Pietenpol, J. A. (2008) A gene signature-based approach identifies mTOR as a regulator of p73. *Mol. Cell. Biol.* **28,** 5951–5964
18. Riedel, R. F., Porrello, A., Pontzer, E., Chenette, E. J., Hsu, D. S., Balakumaran, B., Potti, A., Nevins, J., and Febbo, P. G. (2008) A genomic approach to identify molecular pathways associated with chemotherapy resistance. *Mol. Cancer Ther.* **7,** 3141–3149
19. Iwabuchi, T., Maruyama, T., Sei, Y., and Adachi, K. (1995) Effects of immunosuppressive peptidyl-prolyl cis-trans isomerase (PPIase) inhibitors, cyclosporin A, FK506, ascomycin and rapamycin, on hair growth initiation in mouse: immunosuppression is not required for new hair growth. *J. Dermatol. Sci.* **9,** 64–69
20. Muller-Rover, S., Handjiski, B., van der Veen, C., Eichmuller, S., Foitzik, K., McKay, I. A., Stenn, K. S., and Paus, R. (2001) A comprehensive guide for the accurate classification of murine hair follicles in distinct hair cycle stages. *J. Invest. Dermatol.* **117,** 3–15
21. Christensen, A. V., Arnt, J., and Svendsen, O. (1985) Pharmacological differentiation of dopamine D-1 and D-2 antagonists after single and repeated administration. *Psychopharmacol. Suppl.* **2,** 182–190
22. Prozialeck, W. C., and Weiss, B. (1982) Inhibition of calmodulin by phenothiazines and related drugs: structure-activity relationships. *J. Pharmacol. Exp. Ther.* **222,** 509–516
23. Gafter-Gvili, A., Sredni, B., Gal, R., Gafter, U., and Kalechman, Y. (2003) Cyclosporin A-induced hair growth in mice is associated with inhibition of calcineurin-dependent activation of NFAT in follicular keratinocytes. *Am. J. Physiol. Cell. Physiol.* **284,** C1593–C1603
24. Mammucari, C., Tommasi di Vignano, A., Sharov, A. A., Neilson, J., Havrda, M. C., Roop, D. R., Botchkarev, V. A., Crabtree, G. R., and Dotto, G. P. (2005) Integration of Notch 1 and calcineurin/NFAT signaling pathways in keratinocyte growth and differentiation control. *Dev. Cell* **8,** 665–676
25. Horsley, V., Aliprantis, A. O., Polak, L., Glimcher, L. H., and Fuchs, E. (2008) NFATc1 balances quiescence and proliferation of skin stem cells. *Cell* **132,** 299–310
26. Olschewski, H., Simonneau, G., Galie, N., Higenbottam, T., Naeije, R., Rubin, L. J., Nikkho, S., Speich, R., Hoeper, M. M., Behr, J., Winkler, J., Sitbon, O., Popov, W., Ghofrani, H. A., Manes, A., Kiely, D. G., Ewert, R., Meyer, A., Corris, P. A., Delcroix, M., Gomez-Sanchez, M., Siedentop, H., and Seeger, W. (2002) Inhaled iloprost for severe pulmonary hypertension. *N. Engl. J. Med.* **347,** 322–329

Received for publication September 7, 2009.
Accepted for publication November 25, 2009.

Journal of Dermatological Science 53 (2009) 120–128

Contents lists available at ScienceDirect

Journal of Dermatological Science

journal homepage: www.intl.elsevierhealth.com/journals/jods

Adjuvant effect of lipopolysaccharide on the induction of contact hypersensitivity to haptens in mice

Shoko Yokoi, Hironori Niizeki *, Hideyuki Iida, Hideo Asada, Sachiko Miyagawa

Department of Dermatology, Nara Medical University, Kashihara, Nara, Japan

ARTICLE INFO

Article history:
Received 28 December 2007
Received in revised form 12 August 2008
Accepted 13 August 2008

Keywords:
Toll-like receptor 4
Langerhans cell
TNF-alpha

ABSTRACT

Background: Toll-like receptor (TLR) 4 is a critical receptor and signal transducer for lipopolysaccharide (LPS), a major component of Gram-negative bacteria. The MyD88-independent pathway downstream of TLR4 leads to functional dendritic cell (DC) maturation, although LPS-induced cytokine production from DCs is MyD88-dependent.

Objectives: We investigated whether intracutaneously injected LPS alters the functions of cutaneous DCs, leading to enhanced contact hypersensitivity (CH).

Methods: The ear swelling response was measured to evaluate the magnitude of CH. Cell proliferation of allogeneic splenocytes stimulated by DC-enriched draining lymph node (LN) cells was measured by performing a [^{3}H]-thymidine incorporation assay. Epidermal I-A+ cells were evaluated under an epifluorescent microscope. I-A+ FITC-bearing cells from the draining LNs 24 h after FITC application were analyzed on FACScan.

Results: LPS augmented CH induction in C3H/HeN (HeN) and MyD88-knockout (KO) mice but not in C3H/HeJ (HeJ) and H-2S^d-bearing strains such as BALB/c mice. LPS failed to augment the allo-stimulatory ability of DCs in the draining LNs after hapten applications. LPS altered the density and morphology of epidermal I-A+ cell in HeN and BALB/c mice but not in TLR4-deficient HeJ mice. LPS increased the proportion of I-A+ FITC-bearing cells in the LNs 24 h after FITC application in HeN, but not in BALB/c and HeJ.

Conclusions: LPS augments the ability of DCs to migrate to the draining LNs, leading to enhanced CH via a TLR4-dependent, MyD88-independent pathway. The different effects of LPS on CH in some strains of mice may explain individual differences in the susceptibility to establish CH to daily antigen exposures in clinical settings.

1. Introduction

Contact hypersensitivity (CH) is a T cell dependent immune response, which is induced by the application of haptens on the skin. Dendritic cells (DCs) are the most potent antigen presenting cells and play major roles in the initiation and regulation of adaptive immune responses to antigens [1]. Cutaneous DCs first capture antigens and then migrate to draining lymph nodes (LNs). During migration, cutaneous DCs undergo maturation, which includes the expression of costimulatory molecules and delivery of major histocompatibility complex antigens to their surface. The mature migratory DCs then activate the naïve T cells present in draining LNs or transfer the antigens to resident DCs [2]. Therefore, cutaneous DCs are very important for the determination of the quality and quantity of CH.

Toll-like receptors (TLRs) are the main innate immune sensors. Each TLR responds to specific molecules of microbial origin. Stimulation of different TLRs induces distinct patterns of gene expression, which not only leads to the activation of innate immunity but also induces the development of antigen-specific acquired immunity [3].

Lipopolysaccharide (LPS) is a major component of the outer membranes of Gram-negative bacteria and induces a variety of biological responses including cytokine production from macrophages, B cell proliferation, and endotoxin shock. TLR4 is essential for recognizing LPS because LPS-mediated cytokine release is abrogated in mice having natural mutation of TLR4 or its target disruption [4]. TLR4 is expressed on monocyte-derived DCs. Stimulation of TLR4 on DCs induces interleukin (IL)-12 production, enhances surface expression of costimulatory molecules, and

* Corresponding author at: Present address: Department of Dermatology, National Center for Child Health and Development, 2-10-1 Ohkura, Setagaya, Tokyo, Japan. Tel.: +81 3 3416 0181; fax: +81 3 5494 7136.
E-mail address: niizeki-h@ncchd.go.jp (H. Niizeki).

0923-1811/$30.00 © 2008 Japanese Society for Investigative Dermatology. Published by Elsevier Ireland Ltd. All rights reserved.
doi:10.1016/j.jdermsci.2008.08.009

finally, leads to DC maturation [5]. Moreover, Kaisho et al. [6] reported that the MyD88-independent pathway, downstream of TLR4 could lead to functional DC maturation because LPS could induce functional maturation of the MyD88-deficient DCs, although LPS-induced cytokine production from DCs was MyD88-dependent.

In this study, we determined whether intracutaneously injected LPS could alter the functions of cutaneous DCs and lead to enhanced CH.

2. Materials and methods

2.1. Mice

We purchased adult mice aged 8–12 weeks of the BALB/c, B10.A, B10.D2, C3H/HeN, C3H/HeJ and C57BL/6 strains from Japan SLC, Inc. (Hamamatsu, Shizuoka, Japan). MyD88-knock out (KO) mice were kindly provided by Prof. Akira at the Research Institute for Microbial Diseases, Osaka University [7]. They were maintained in our animal facility with SPF environment. Experimental procedures were carried out with animals under general anesthesia achieved by intraperitoneal (i.p.) injections of ketamine (Sankyo, Tokyo, Japan) (80 mg/kg) and xylazine (Bayer Healthcare, Leverkusen, Germany) (16 mg/kg) or pentobarbitone (Dainippon-Sumitomo, Osaka, Japan) (50 mg/kg). Animal care was in accordance with the guidelines of Nara Medical University. Each control or experimental panel consisted of 4–5 mice.

2.2. Reagents

LPS from *Escherichia coli* 026:B6, fluorescein isothiocyanate (FITC), and 2,4-dinitro-1-fluorobenzene (DNFB) were purchased from Sigma–Aldrich (St. Louis, MO). Anti-mouse tumor necrosis factor (TNF)-α/TNFSF1A antibodies (Abs) and normal goat IgG were purchased from Genzyme/Techne (Minneapolis, MN). Anti-I-A^k, I-A^d monoclonal antibodies (mAbs), and isotype-matched control Abs were purchased from BD Pharmingen (San Diego, CA).

2.3. Intradermal injection

Using a 1.0 ml syringe with a 30-gauge needle, the solution was injected into the intradermal (i.d.) space. Successful inoculations were characterized by the appearance of a flat swelling with defined lateral margins immediately beneath the epidermis [8].

2.4. Induction and expression of CH

On day 0, 25 μl of 0.5% DNFB (185 μg) in acetone was applied on the dry-shaved abdominal cutaneous surface of mice. On day 5, CH was elicited by challenging one ear of each mouse with 20 μl of 0.05% DNFB (15 μg). Ear swelling was measured using an engineer's micrometer (Mitutoyo, Kawasaki, Kanagawa, Japan) 24 and 48 h following the challenge and compared with the thickness of ear prior to the challenge [8–11].

2.5. Identification and enumeration of epidermal DCs

The epidermis was separated from the dermis by incubation in Dispase II (Roche Diagnostics GmbH, Mannheim, Germany). DCs in these epidermal sheets were stained with anti-I-A mAbs (BD Pharmingen) and FITC-tagged goat anti-mouse Abs (Zymed, South San Francisco, CA), as described previously [9], and evaluated under an epifluorescence microscope. With the aid of an eyepiece with a 1 mm^2 grid, a minimum of 10 fields were counted for each sample to enumerate the number of positively stained cells present, and the mean number of stained cells was expressed as cells/mm^2.

2.6. Mixed lymphocyte reaction

The axillary and inguinal LNs were excised 5 days after applying 25 μl of 0.5% DNFB on the abdominal skin of mice. The LNs were gently disrupted to yield a single cell suspension and filtered through 70-μM nylon meshes (BD FALCON™). DC population was enriched with the Mouse DC Enrichment Kit (DYNAL®) according to the manufacturer's instructions. The purity of DCs was assessed under an epifluorescent microscope after staining with anti-I-A-PE mAbs (BD Pharmingen) and estimated to be 50–70%. The enriched DCs were X-irradiated (2.9 G) and washed three times with phosphate-buffered saline (PBS) containing 2% fetal bovine serum (FBS). Spleens were harvested from naïve allogeneic mice (BALB/c, H-2^d) and filtered through 100-μM nylon meshes. The erythrocytes were lysed using the mouse erythrocyte lysing kit (R&D Systems). A total of 2×10^5 splenocytes were co-cultured with various numbers of prepared X-irradiated LN cells in RPMI medium supplemented with 10% heat-inactivated FBS (Sigma–Aldrich), 0.1 mM non-essential amino acids (Gibco, Grand Island, NY), 2 mM L-glutamine (Gibco), 25 mM HEPES buffer (Sigma–Aldrich), and 1% penicillin–streptomycin (Gibco) in round-bottomed 96-well plates at 37 °C. Five days after co-culture, all wells were pulsed with 1 μCi of [^{3}H]-thymidine for an additional 16–18 h of culture. The cells were then harvested, and [^{3}H]-thymidine incorporation was measured by liquid scintillation counting [12].

2.7. Immunofluorescent staining and flow cytometry

On the shaved abdominal skin of HeN and HeJ mice, we applied 400 μl of 0.5% FITC in 1:1 acetone/dibutyl phthalate. Mice were sacrificed 48 h later and the axillary and inguinal LNs were excised. The LNs were gently disrupted to yield a single cell suspension and filtered through 70-μM nylon meshes. The cells were collected, washed three times with PBS with 2% FBS. To enrich for DC, LN cells were suspended in RPMI, and then 5 ml of the cell suspension was gently underlaid with 4 ml of Nycoprep TM (Oslo, Norway), followed by centrifugation at 300 × *g* for 20 min. The cells at the interface were collected, washed three times with PBS with 2% FBS. Cells were stained with phycoerythin (PE)-conjugated anti-I-A^k or I-A^d mAb, diluted 1/1000 or isotype-matched control Ab for 30 min on ice, and washed three times with PBS containing 1% bovine serum albumin (BSA) and 0.1% sodium azide. Propidium iodine (PI, 1%) (Sigma–Aldrich) was used to identify the dead cells [13]. The stained cells were analyzed on FACScan with the CellQuest software™ (Becton Dickinson Immunocytometry Systems, San Jose, CA).

2.8. Statistical analysis

The statistical significance of differences between the means of the each experimental group was determined using Student's *t* test. The mean differences were considered significant at $P < 0.05$. Each experiment was performed at least twice.

3. Results

3.1. LPS augments the induction of CH

We first examined the effect of LPS on the induction of CH. LPS (25 and 5 μg) or PBS was injected (i.d.) into panels of C3H/HeN (HeN), C3H/HeJ (HeJ), and BALB/c mice. Within 30 min, 185 μg DNFB was applied on the cutaneous surface of the injected sites.

Five days later, the ears of these mice were challenged with 15 μg DNFB and the ear swelling responses measured after 24 and 48 h. The results of a representative experiment are shown in Fig. 1A–C. When DNFB was applied on the PBS-injected skin (positive control), intense CH was induced. However, when DNFB was applied on LPS-injected skin, the HeN recipients mounted further intense CH responses than the positive control mice upon ear challenge (Fig. 1A). The intensity of CH in the skin injected previously with 25 μg LPS was not significantly enhanced compared with that in the skin injected with 5 μg LPS. Thus, in HeN mice, injection of LPS into the skin significantly intensified the ability of DNFB-applied skin to induce CH. In contrast, when LPS was injected intradermally in the TLR4-sufficient BALB/c mice (Fig. 1B) and TLR4-deficient HeJ mice (Fig. 1C), the magnitude of CH was similar to that in the positive control. Each experiment was repeated at least twice with very similar results. We thus conclude that TLR4 mediates the effect of LPS on the induction of CH in HeN mice. In addition, it is suggested that BALB/c mice, in which TLR4 is sufficiently expressed, are a resistant strain with regard to the effect of LPS on the CH induction. This indicates that not only TLR4 but also another factor such as TNF-α may determine the susceptibility to LPS (14).

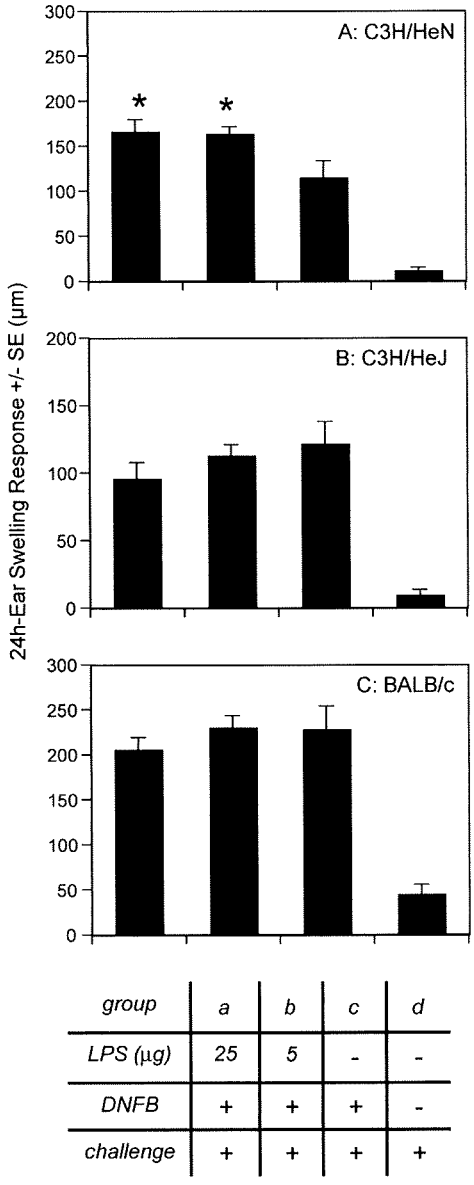

Fig. 1. LPS augments the induction of CH in C3H/HeN mice. Panels of C3H/HeN (A), BALB/c (B), and C3H/HeJ mice (C) were injected intradermally with 25 μg LPS (a), 5 μg LPS (b), and PBS (c), respectively. Within 30 min, 185 μg DNFB was applied at the injected sites. Five days later, the ears were challenged with DNFB. Unsensitized animals were also challenged and used as negative controls (d). Ear swelling responses at 24 h are presented as mean ± S.E.M. (μm). $^{*}P < 0.05$ versus PBS (positive control).

3.2. H-2 linked to susceptibility to the effect of LPS on CH induction

We next determined whether susceptibility to the effect of LPS on CH induction is H-2 dependent. Previous studies in mice have indicated that the UVB-susceptibility trait is related to the class III region in the H-2 complex (14). Because BALB/c strain has an H-2^d genetic background, we chose B10.D2 and B10.A as B10-congenic inbred strains that carry H-2^d haplotype (Table 1).

LPS (25 μg) or PBS was injected intradermally into panels of mice. Within 30 min, 185 μg DNFB was applied on the cutaneous surface of the injected sites. After 5 days, the ears of these mice were challenged with 15 μg DNFB, and the ear swelling responses were measured after 24 and 48 h. The results of a representative experiment are shown in Fig. 2A and B. When DNFB was applied on the PBS-injected skin (positive control), intense CH was induced. However, when LPS was injected intradermally in the H-2^d-bearing B10.A mice (Fig. 2A) and B10.D2 mice (Fig. 2B), the magnitude of CH was similar to that in the positive control. Thus, the adjuvant effect of LPS on CH induction is H-2 dependent; k and b of H-2 are susceptible traits and d of H-2 is a resistant trait.

3.3. The augmentation of CH by LPS is MyD88-independent

We next determined whether the effect of LPS on CH is MyD88-dependent because TLR4 mediates the adjuvant effect of LPS on the induction of CH.

Panels of MyD88-KO littermates and their wild-type counterparts (B6 background) were administered (i.d.) LPS (25 μg/mouse) or PBS. Within 30 min, 185 μg DNFB was applied on the epidermis of the injected sites. Five days later, the ears of these mice were challenged with 15 μg DNFB and the ear swelling response measured after 24 and 48 h. The results of a representative experiment are shown in Fig. 3. Unsensitized animals were also challenged and used as negative controls (Fig. 3, groups c and f). When DNFB was applied on the skin on LPS-injected mice (group d), the wild-type recipients (wild) mounted more intense CH responses than the positive control mice (group e). Similarly, the MyD88-KO recipients (KO) in which LPS had been injected previously (group a) mounted more intense CH responses than the positive control mice (group b). Thus, these data suggest that

Table 1
Genetic background and LPS susceptibility in mice [14]

	Locus			
Strain	Ea	Tnfa	D	phenotype
C57BL/6	b	b	b	susceptible
C3H/HeN	k	k	k	susceptible
BALB/c	d	d	d	resistant
B10.D2	d	d	d	resistant
B10.A	k	d	d	resistant

Gray box indicates LPS resistant mice and their H-2 alleles.